

Equilibrium transport with time-inconsistent costs: An application to matching problems in the job market

Erhan Bayraktar ^{*} Bingyan Han [†]

August 28, 2023

Abstract

Given two probability measures on sequential data, we investigate the transport problem with time-inconsistent preferences under a discrete-time setting. Motivating examples are nonlinear objectives, state-dependent costs, and regularized optimal transport with general f -divergence. Under the bicausal constraint, we introduce the concept of equilibrium transport. The existence is proved in the semi-discrete Markovian case and the continuous non-Markovian case with strict quasiconvexity, while the uniqueness also holds in the second case. We apply our framework to study inertia of two job markets, top-ranking executives and academia. The empirical analysis shows that a job market with stronger inertia is less efficient. The University of California (UC) postdoc job market has the strongest inertia even than that of executives, while there is no evidence of inertia in the UC faculty job market.

Keywords: Dynamic programming; time-inconsistent costs; bicausal optimal transport; job market

1 Introduction

Optimal transport (OT) is a method for quantifying the discrepancy between two probability distributions. The origins of OT can be traced back to Monge’s mass transfer problem in the 18th century. However, it was not until the advent of linear programming in the mid 20th century that OT was revitalized by Kantorovich. In the 1990s, Brenier (1991) and Gangbo and McCann (1996) provided new insights into OT through the lens of convex analysis and geometry. Nowadays, OT is recognized as an interdisciplinary tool with a wide range of applications in fields such as mathematics (Villani, 2009), machine learning (Arjovsky et al., 2017; Peyré and Cuturi, 2019), economics (Galichon, 2016), statistics (Torous et al., 2021), biology (Schiebinger et al., 2019), operations research (OR), and management science (MS).

A major application of OT in OR/MS is robust optimization. Many decision-making tasks are based on a nominal probability measure, which may not be accurate. Wasserstein distances were used in distributionally robust optimization by considering alternative measures within a certain Wasserstein distance from the nominal distribution and selecting decision rules that perform well even in the worst-case scenario (Blanchet and Murthy, 2019; Blanchet et al., 2021a; Gao and

^{*}Department of Mathematics, University of Michigan, Ann Arbor, Email: erhan@umich.edu. Erhan Bayraktar is partially supported by the National Science Foundation under grant DMS-2106556 and by the Susan M. Smith chair.

[†]Department of Mathematics, University of Michigan, Ann Arbor. Email: byhan@umich.edu.

Kleywegt, 2022; Mohajerin Esfahani and Kuhn, 2018; Nguyen et al., 2022; Kuhn et al., 2019; Blanchet et al., 2021b).

The OT theory also finds applications in quantitative economics. OT is motivated by resource allocation problems in economics, for which Kantorovich shared the Nobel Prize in Economics with Koopmans in 1975. The duality theory in OT can be linked to a welfare theorem (Galichon, 2016, Chapter 3), with applications in family economics including marriage market analysis. The hedonic model is a variant of OT, as evidenced by Carlier and Ekeland (2010); Chiappori et al. (2010). Additionally, the Monge–Kantorovich problem connects to gravity equations in international trade and discrete choice models in economics; see Taşkesen et al. (2023); Galichon (2016). Furthermore, Section 5.1 shows the equivalence between a CEO compensation model (Gabaix and Landier, 2008) and the OT problem.

While most literature on OT has focused on static data without a chronological structure, temporal data are ubiquitous in finance, statistics, and optimization. To address this, Lassalle (2013) introduced causal optimal transport (COT), which imposes a causality constraint on the transport plans between discrete stochastic processes. In a less formal sense, COT requires that when the past of one process, X , is given, the past of another process, Y , should be independent of the future of X under the transport plan. COT has found applications in mathematical finance (Backhoff-Veraguas et al., 2020), video modeling (Xu et al., 2020), mean-field games (Acciaio et al., 2021; Backhoff-Veraguas and Zhang, 2023), and stochastic optimization (Pflug and Pichler, 2012, 2014; Acciaio et al., 2020).

When making decisions over time, humans often exhibit time inconsistency, where the optimal plan at the present moment is not followed in the future. To address this, consistent planning is suggested as a remedy by Strotz (1955). Time inconsistency is observed in non-exponential discounting (Strotz, 1955; Laibson, 1997), prospect theory (Kahneman and Tversky, 1979), gambling behaviors (Barberis, 2012), and classical mean-variance portfolio selection (Basak and Chabakauri, 2010). Mathematical models with time inconsistency include variants of portfolio selection (Björk and Murgoci, 2014; Björk et al., 2014, 2017; Han et al., 2021; Kováčová and Rudloff, 2021), optimal stopping (Bayraktar et al., 2021; Pichler et al., 2022), robust decision-making (Epstein and Ji, 2022; Arora and Gao, 2022), probability distortion (Ma et al., 2021), and risk measures in Pflug and Pichler (2014, Chapter 5) and Föllmer and Schied (2011, Chapter 11).

In this paper, we generalize the classical Monge-Kantorovich problem to a dynamic setting with time-inconsistent costs. Suppose transport plans are bicausal in the sense that two processes are causal with respect to each other. The cost function is allowed to include time-inconsistent preferences such as nonlinear objectives and state dependence. Moreover, we notice that regularization with general f -divergence (Bayraktar et al., 2022; Taşkesen et al., 2023) can also be a new source of time inconsistency. To address the self-contradictory behavior and the violation of dynamic programming principle (henceforth DPP), we adopt the subgame Nash equilibria solution as in Björk and Murgoci (2014); Basak and Chabakauri (2010). This concept, given formally in Definition 2.1, is well-defined and easy to understand in a discrete-time setting. Our first main contribution is the characterization of the equilibrium transport under an extended DPP. Theorem 3.3 and Corollary 3.5 show the existence of the equilibrium transport under a semi-discrete setting with Markovian dynamics. The refining topology idea is new in the proof of DPP. Theorem 4.4 proves the existence and uniqueness under the continuous and non-Markovian setting with a strict quasiconvexity assumption and parametric couplings. As a simple application, a concrete example illustrating Theorem 4.4 is given in Section 4.2.1.

Our framework introduces a new methodology with a wide range of potential interdisciplinary applications. Motivated by the OT applications in economics (Galichon, 2016), we consider the matching between employers and employees, quantified by firm net sales and wages. This problem

has been studied extensively for the labor market of top executives (Gabaix and Landier, 2008; Demerjian et al., 2012; Taylor, 2013). A stylized empirical effect, known as Roberts’ law in Gabaix and Landier (2008), states that larger firms pay more to top executives represented by chief executive officers (CEOs). This firm-wage matching is also called positive assortative matching (PAM), where firms ranked number n in terms of sizes (net sales or market values) should pay qualified executives with wages ranked number n . However, empirical data do not always show a perfect correspondence between firm sizes and wages. This raises questions why PAM may fail and some high-ranked firms pay less to executives.

We conjecture that there are incentives for firms to maintain similar firm-wage matching over time, regardless of whether it aligns with PAM or not. These incentives can stem from regulatory requirements, momentum in financial performance, and status quo bias. Regulators require public companies to provide a year-over-year comparison of executive compensations, implying that regulators and stakeholders want to detect abnormal changes in wages. Additionally, wages are often tied to financial performance, such as stock prices, which may also exhibit momentum. Furthermore, people tend to keep the current situation stable and may be resistant to change, leading to a status quo bias in the firm-wage matching. Motivated by these factors, in Section 5, we propose a novel job market model that incorporates a state-dependent term capturing the potential persistence or inertia of maintaining previous matching over time. This allows us to quantify the underlying incentives that contribute to the observed patterns in the labor market.

We call a job market more efficient if it is more consistent with the Roberts’ law. Through our empirical analysis in Sections 6 and 7, we find that a job market is less efficient when its inertia represented by state dependence is stronger. Specifically, over the last five years, the Consumer Discretionary, Real Estate, and Information Technology industries have the weakest correlations between net sales and wages, while they exhibit stronger inertia or state dependence. In addition to the well-studied executive job market, we also examine the academic job market which received less attention in the literature.

Thanks to the Transparent California project, we are able to analyze wage data from the University of California (UC) system. In Section 7, wages for faculty in Business, Economics, and Engineering departments, including full professors, associate professors, and assistant professors, are found to be almost perfectly consistent with U.S. News National University Rankings. There is no evidence of any inertia for faculty wages. However, we find that the median wages of postdocs from all departments are highly inconsistent with university rankings. The state dependence or inertia in the postdoc job market is even stronger than that of top executives in any industry. In contrast to the attention on executive compensation, the inefficiency and inertia in the postdoc job market are rarely discussed in the literature.

Our paper also offers practical techniques to enhance the robustness of the results. In Section 6.2.1, we adopt a data-driven method to determine the optimal number of clusters in the discretization of the OT algorithm. Additionally, in Section 6.2.3, we employ a model validation procedure by testing the model with synthetic perfectly matched firm-wage paths. Besides, we utilize the bootstrapping technique for data augmentation. These procedures ensure that our findings are robust across multiple simulation runs and varying numbers of clusters, despite the inherent noise in the net sale and wage data. The Python code is publicly available on the GitHub repository: <https://github.com/hanbingyan/equitrans>.

The rest of the paper is organized as follows. We introduce the usual weak topology and bicausal OT in Sections 1.1 and 1.2. Section 2 presents motivations for equilibrium transport and characterization with extended DPP in the discrete case. Section 3 considers the semi-discrete and Markovian case. Section 4 presents the continuous and non-Markovian case. Section 5 introduces a new job market model with inertia measured by state dependence. Sections 6 and 7 apply the

model to executive and academic job markets. Technical proofs are deferred to Section A in the e-companion. Sections B and C in the e-companion give some supplementary Tables and Figures.

1.1 Notation and the usual weak topology

Denote the finite number of periods as T . For each $t \in \{1, \dots, T\}$, consider a Polish (complete, separable, and metrizable) space $(\mathcal{X}_t, \mathcal{T}_{\mathcal{X}_t})$, where \mathcal{X}_t is a closed (but not necessarily bounded) subset of \mathbb{R}^d . \mathcal{X}_t is interpreted as the range of the process at time t . Let $C(\mathcal{X}_t; \mathcal{T}_{\mathcal{X}_t})$ be the set of continuous functions $f : (\mathcal{X}_t, \mathcal{T}_{\mathcal{X}_t}) \rightarrow (\mathbb{R}, \mathcal{T}_{\mathbb{R}})$, where \mathbb{R} is always equipped with the usual topology $\mathcal{T}_{\mathbb{R}}$. $C_b(\mathcal{X}_t; \mathcal{T}_{\mathcal{X}_t})$ is the set of continuous and bounded functions. Denote $\mathcal{B}(\mathcal{T}_{\mathcal{X}_t})$ as the Borel σ -algebra of the topological space $(\mathcal{X}_t, \mathcal{T}_{\mathcal{X}_t})$.

In this paper, we always endow the product space with the product topology. $\mathcal{X}_{1:T} := \mathcal{X}_1 \times \dots \times \mathcal{X}_T$ is a closed subset of $\mathbb{R}^{T \times d}$ with the product topology $\mathcal{T}_{\mathcal{X}} := \prod_{t=1}^T \mathcal{T}_{\mathcal{X}_t}$, which is also Polish. With some abuse of notation, we simply write \mathcal{X} while we mean $\mathcal{X}_{1:T}$. By Kallenberg (2021, Lemma 1.2), the Borel σ -algebra of the product space satisfies $\mathcal{B}(\mathcal{X}) = \mathcal{B}(\mathcal{X}_1) \otimes \dots \otimes \mathcal{B}(\mathcal{X}_T)$.

Denote the set of all Borel probability measures on \mathcal{X} as $\mathcal{P}(\mathcal{X})$. As in Bertsekas and Shreve (1978, Section 7.4.2) and Parthasarathy (2005, Section II.6), the usual weak topology is defined as follows. For a given $\varepsilon > 0$, $\mu \in \mathcal{P}(\mathcal{X})$, and $f \in C_b(\mathcal{X}; \mathcal{T}_{\mathcal{X}})$, define the subset of $\mathcal{P}(\mathcal{X})$ as

$$V(\mu; f, \varepsilon) := \left\{ \mu' \in \mathcal{P}(\mathcal{X}) : \left| \int f d\mu - \int f d\mu' \right| < \varepsilon \right\}.$$

Consider the collection of these subsets as

$$V[C_b(\mathcal{X}; \mathcal{T}_{\mathcal{X}})] := \{V(\mu; f, \varepsilon) : \varepsilon > 0, \mu \in \mathcal{P}(\mathcal{X}), f \in C_b(\mathcal{X}; \mathcal{T}_{\mathcal{X}})\}.$$

We endow $\mathcal{P}(\mathcal{X})$ with $\mathcal{V}[C_b(\mathcal{X}; \mathcal{T}_{\mathcal{X}})]$, the weakest topology on $\mathcal{P}(\mathcal{X})$ which contains the collection $V[C_b(\mathcal{X}; \mathcal{T}_{\mathcal{X}})]$. By Parthasarathy (2005, Theorems 6.2 and 6.5), $(\mathcal{P}(\mathcal{X}), \mathcal{V}[C_b(\mathcal{X}; \mathcal{T}_{\mathcal{X}})])$ is a Polish topological space if and only if $(\mathcal{X}, \mathcal{T}_{\mathcal{X}})$ is so.

In the OT theory, we need to consider another closed set $\mathcal{Y} = \mathcal{Y}_{1:T} = \mathcal{Y}_1 \times \dots \times \mathcal{Y}_T$. We also equip each factor space \mathcal{Y}_t with a Polish topology $\mathcal{T}_{\mathcal{Y}_t}$ and other notations are introduced similarly as in the counterparts for \mathcal{X} .

For notational convenience, we interpret $\mathcal{X}_{1:t}$, $\mathcal{X}_{1:t} \times \mathcal{Y}_{1:t}$, and other similar terms as the product of factor spaces with indices in $1, \dots, t$. For a Borel probability measure μ on temporal data, we denote $\mu(dx_{t+1:T}|x_{1:t})$ as a regular conditional probability kernel of $x_{t+1:T}$ given $x_{1:t}$, which is uniquely determined in a suitable way (Bogachev, 2007, Theorem 10.4.14 and Corollary 10.4.17). When there is no confusion, we also write the kernel as μ^t for simplicity. If μ is a finite discrete measure, we sometimes use $\mu(x_{t+1:T}|x_{1:t})$, which omits the differential, as the conditional probability at the atom $x_{t+1:T}$ given $x_{1:t}$. The initial state at time 0 is always fixed.

We emphasize that metrics and Wasserstein distances are introduced for the continuous case in Section 4 only. The semi-discrete case in Section 3 does not rely on a specific choice of the metric.

1.2 Bicausal optimal transport

There is a vast literature on the OT theory and its applications (Villani, 2009; Kuhn et al., 2019; Blanchet et al., 2021b). However, the previous works have been focusing on data without the time dimension. Motivated by the ubiquitous role of temporal data in OR/MS, finance, and economics, a new notion of adapted Wasserstein distance or causal optimal transport (COT) has been proposed to compare distributions on temporal data (Lassalle, 2013; Backhoff-Veraguas et al., 2017). We present a brief review in this subsection as a self-contained article.

Consider two probability measures $\mu \in \mathcal{P}(\mathcal{X})$ and $\nu \in \mathcal{P}(\mathcal{Y})$. Denote $\Pi(\mu, \nu)$ as the set of all the couplings that admit μ and ν as marginals. Suppose transporting one unit of mass from x to y incurs a cost of $c(x, y)$. A generic OT problem is formulated as

$$\mathcal{W}(\mu, \nu) := \inf_{\pi \in \Pi(\mu, \nu)} \int_{\mathcal{X} \times \mathcal{Y}} c(x, y) \pi(dx, dy).$$

If the data have a temporal structure as $x = (x_1, \dots, x_t, \dots, x_T)$ and $y = (y_1, \dots, y_t, \dots, y_T)$, not all couplings $\pi \in \Pi(\mu, \nu)$ will make sense. A natural requirement of the transport plan $\pi(x, y)$ should be the non-anticipative condition. Informally speaking, if the past of x is given, then the past of y should be independent of the future of x under the measure π . Mathematically, it means a transport plan π should satisfy

$$\pi(dy_t | dx_{1:T}) = \pi(dy_t | dx_{1:t}), \quad t = 1, \dots, T-1, \quad \pi\text{-a.s.} \quad (1.1)$$

The property (1.1) is known as the causality condition from x to y and the transport plan satisfying (1.1) is called *causal* by Lassalle (2013). It can be interpreted by the equivalent formulation: $y_t = F_t(x_{1:t}, U_t)$, $\forall t \in 1, \dots, T$, for some measurable functions F_t and uniform random variables U_t . Crucially, U_t is independent of $x_{1:T}$, but the $\{U_t\}_{t=1}^T$ need not to be independent of each other; see Kallenberg (2021, Theorem 8.17) and Backhoff-Veraguas et al. (2017).

If (1.1) holds when we exchange the positions of x and y , then the transport plan is called bicausal. Denote $\Pi_{bc}(\mu, \nu)$ as the set of all bicausal transport plans between μ and ν . The bicausal OT problem considers the optimization over $\Pi_{bc}(\mu, \nu)$ only:

$$\mathcal{W}_{bc}(\mu, \nu) := \inf_{\pi \in \Pi_{bc}(\mu, \nu)} \int_{\mathcal{X} \times \mathcal{Y}} c(x, y) \pi(dx, dy). \quad (1.2)$$

For applications of (bi)causal optimal transport, see Backhoff-Veraguas et al. (2020); Xu et al. (2020); Acciaio et al. (2021); Pflug and Pichler (2012); Acciaio et al. (2020) for an incomplete list.

In this paper, we consider two probability measures μ and ν with symmetric positions and focus on the bicausal transport plans only. For a given transport plan $\pi \in \Pi(\mu, \nu)$, we can decompose π in terms of successive regular kernels:

$$\begin{aligned} \pi(dx_{1:T}, dy_{1:T}) = & \bar{\pi}(dx_1, dy_1) \pi(dx_2, dy_2 | x_1, y_1) \pi(dx_3, dy_3 | x_{1:2}, y_{1:2}) \dots \\ & \pi(dx_T, dy_T | x_{1:T-1}, y_{1:T-1}). \end{aligned} \quad (1.3)$$

By Backhoff-Veraguas et al. (2017, Proposition 5.1), π is a bicausal transport plan if and only if

- (1) $\bar{\pi} \in \Pi(p_*^1 \mu, p_*^1 \nu)$, and
- (2) for each $t = 1, \dots, T-1$ and π -almost every path $(x_{1:t}, y_{1:t})$, the following condition holds:

$$\pi(dx_{t+1}, dy_{t+1} | x_{1:t}, y_{1:t}) \in \Pi(\mu(dx_{t+1} | x_{1:t}), \nu(dy_{t+1} | y_{1:t})).$$

$p_*^1 \mu$ (resp. $p_*^1 \nu$) is the pushforward of μ (resp. ν) by the projection p^1 onto the first coordinate.

2 Equilibrium transport

Time-consistent problems satisfy the Bellman equation. If a solution is optimal on the time interval $\{t, \dots, T-1\}$, then it is also optimal on any subinterval $\{s, \dots, T-1\}$ with $s \geq t$. However, there are various time-inconsistent preferences (Strotz, 1955; Kahneman and Tversky, 1979; Laibson, 1997; Basak and Chabakauri, 2010). In this context, we present three instances where time inconsistency arises in the bicausal OT problem, with the regularization case being particularly noteworthy and previously unnoticed.

2.1 Motivation

2.1.1 Regularized bicausal OT

In practice, continuous densities are approximated by empirical measures with finite supports. The computational burden of discrete OT can be high, then regularization is adopted in implementation (Cuturi, 2013). The discrete bicausal OT with regularization is

$$\inf_{\pi \in \Pi_{bc}(\mu, \nu)} \langle c(x_{1:T}, y_{1:T}), \pi(x_{1:T}, y_{1:T}) \rangle_F + \left\langle f \left(\frac{\pi(x_{1:T}, y_{1:T})}{\mu(x_{1:T}) \otimes \nu(y_{1:T})} \right), \mu(x_{1:T}) \otimes \nu(y_{1:T}) \right\rangle_F \quad (2.1)$$

for a convex function f . The last term is known as the f -divergence. $\langle c(x_{1:T}, y_{1:T}), \pi(x_{1:T}, y_{1:T}) \rangle_F = \sum_{x_{1:T} \in \mathcal{X}, y_{1:T} \in \mathcal{Y}} c(x_{1:T}, y_{1:T}) \pi(x_{1:T}, y_{1:T})$, which sums over all paths. The arguments $(x_{1:T}, y_{1:T})$ in $\langle c(x_{1:T}, y_{1:T}), \pi(x_{1:T}, y_{1:T}) \rangle_F$ should be interpreted as dummy variables similar in the integral (1.2). $\mu \otimes \nu$ is the independent coupling and $\frac{\pi}{\mu \otimes \nu}$ is interpreted as an element-wise division.

A popular choice of $f(\cdot)$ is the Kullback–Leibler (KL) divergence given by $f(x) = x \ln(x)$. In this case, the regularized objective (2.1) is still time-consistent. Indeed, the KL divergence is separable in the sense that

$$\begin{aligned} & \text{KL}(\pi(x_{1:T}, y_{1:T}) \| \mu(x_{1:T}) \otimes \nu(y_{1:T})) \\ &= \left\langle \ln \left(\frac{\pi(x_{1:T}, y_{1:T})}{\mu(x_{1:T}) \otimes \nu(y_{1:T})} \right), \pi(x_{1:T}, y_{1:T}) \right\rangle_F \\ &= \left\langle \left\langle \ln \left(\frac{\pi(x_T, y_T | x_{1:T-1}, y_{1:T-1})}{\mu(x_T | x_{1:T-1}) \otimes \nu(y_T | y_{1:T-1})} \right), \pi(x_T, y_T | x_{1:T-1}, y_{1:T-1}) \right\rangle_F \right. \\ & \quad \left. + \ln \left(\frac{\pi(x_{1:T-1}, y_{1:T-1})}{\mu(x_{1:T-1}) \otimes \nu(y_{1:T-1})} \right), \pi(x_{1:T-1}, y_{1:T-1}) \right\rangle_F. \end{aligned} \quad (2.2)$$

For simplicity, we denote the successive regular kernels of $\pi(x_{1:T}, y_{1:T})$ as $\{\bar{\pi}, \pi_1, \dots, \pi_{T-1}\}$. For example, $\pi_{T-1} = \pi(x_T, y_T | x_{1:T-1}, y_{1:T-1})$. The second equality (2.2) shows that the optimization over π_{T-1} is only determined by the first term. We can repeat the decomposition on the second term recursively over time. The classical DPP is applicable in this setting. If $\{\pi_t^*, \dots, \pi_{T-1}^*\}$ is optimal on the interval $\{t, \dots, T-1\}$, then $\{\pi_s^*, \dots, \pi_{T-1}^*\}$ is also optimal on the subinterval $\{s, \dots, T-1\}$ with $s > t$.

However, the entropic regularization can be numerically unstable and fails to preserve transport plan sparsity, prompting exploration of alternative choices for $f(\cdot)$ as discussed in Bayraktar et al. (2022). Notably, Taşkesen et al. (2023, Proposition 3.5 and Theorem 3.7) proved that some f -divergence regularization in the primal problem is equivalent to the so-called smooth c -transform in the dual problem.

Some non-separable examples with time inconsistency are

- (1) Squared Hellinger distance: $f(x) = (1 - \sqrt{x})^2$. The f -divergence term becomes

$$\left\langle f \left(\frac{\pi(x_{1:T}, y_{1:T})}{\mu(x_{1:T}) \otimes \nu(y_{1:T})} \right), \mu(x_{1:T}) \otimes \nu(y_{1:T}) \right\rangle_F = 2 - 2 \left\langle \sqrt{\pi(x_{1:T}, y_{1:T})}, \sqrt{\mu(x_{1:T}) \otimes \nu(y_{1:T})} \right\rangle_F.$$

- (2) Le Cam distance: $f(x) = \frac{(x-1)^2}{2x+2}$ and

$$\left\langle f \left(\frac{\pi(x_{1:T}, y_{1:T})}{\mu(x_{1:T}) \otimes \nu(y_{1:T})} \right), \mu(x_{1:T}) \otimes \nu(y_{1:T}) \right\rangle_F = \frac{1}{2} \sum_{x_{1:T}, y_{1:T}} \frac{[\pi(x_{1:T}, y_{1:T}) - \mu(x_{1:T}) \otimes \nu(y_{1:T})]^2}{\pi(x_{1:T}, y_{1:T}) + \mu(x_{1:T}) \otimes \nu(y_{1:T})}.$$

The summation is over all possible paths $x_{1:T}$ and $y_{1:T}$.

(3) Jensen-Shannon divergence: $f(x) = x \ln(\frac{2x}{x+1}) + \ln(\frac{2}{x+1})$, and

$$\text{JS}(\mathbb{P}, \mathbb{Q}) = \text{KL}\left(\mathbb{P} \parallel \frac{\mathbb{P} + \mathbb{Q}}{2}\right) + \text{KL}\left(\mathbb{Q} \parallel \frac{\mathbb{P} + \mathbb{Q}}{2}\right),$$

with $\mathbb{P} = \pi$, $\mathbb{Q} = \mu \otimes \nu$ is the independent coupling.

Under these specifications, the objective is no longer separable and the DPP is violated. The cost functional at time t is given by

$$\begin{aligned} J(x_{1:t}, y_{1:t}; \pi) &= \langle c(x_{1:T}, y_{1:T}), \pi(x_{t+1:T}, y_{t+1:T} | x_{1:t}, y_{1:t}) \rangle_F \\ &+ \left\langle f\left(\frac{\pi(x_{t+1:T}, y_{t+1:T} | x_{1:t}, y_{1:t})}{\mu(x_{t+1:T} | x_{1:t}) \otimes \nu(y_{t+1:T} | y_{1:t})}\right), \mu(x_{t+1:T} | x_{1:t}) \otimes \nu(y_{t+1:T} | y_{1:t}) \right\rangle_F. \end{aligned} \quad (2.3)$$

When the iterated expectation relationship (or tower property) fails, a global optimal transport plan on $\{t, \dots, T-1\}$ may not be optimal for the subproblems on $\{t+1, \dots, T-1\}$. The intuition is that we may sacrifice the optimality on the subinterval $\{t+1, \dots, T-1\}$ to attain better solutions on $\{t, \dots, T-1\}$. Nevertheless, an agent can still choose to ignore time inconsistency and follow the global optimizer at time 0 irrevocably. However, he should recognize that the “today self” and “future selves” have an intertemporal conflict with the “optimal” plan (Strotz, 1955).

2.1.2 Nonlinear objectives

With a nonlinear function G , suppose the agent would like to minimize the transport cost given by

$$\inf_{\pi \in \Pi_{bc}(\mu, \nu)} G\left(\int h(x_{1:T}, y_{1:T}) \pi(dx_{1:T}, dy_{1:T})\right).$$

An illustrative example is

$$\inf_{\pi \in \Pi_{bc}(\mu, \nu)} \left(\int h(x_{1:T}, y_{1:T}) \pi(dx_{1:T}, dy_{1:T}) - m\right)^2.$$

The agent wants to match the expected value of $h(\cdot, \cdot)$ to a given level of m . Time inconsistency appears since the tower property fails for the objective.

2.1.3 State-dependent preference

For a fixed $t = 0, \dots, T-1$, consider an objective functional

$$J(x_{1:t}, y_{1:t}; \pi) = \int c(x_t, y_t, x_{1:T}, y_{1:T}) \pi(dx_{t+1:T}, dy_{t+1:T} | x_{1:t}, y_{1:t}). \quad (2.4)$$

The cost c has four arguments. The first (x_t, y_t) is state-dependent and plays a different role than the counterpart in $x_{1:T}$ and $y_{1:T}$. That is, for a different time $s \neq t$, the integrand becomes $c(x_s, y_s, x_{1:T}, y_{1:T})$. Therefore, the integrand is different when the time changes and it leads to time inconsistency.

A classical example is non-exponential discounting (Strotz, 1955; Laibson, 1997). At time t , consider

$$\inf_{\pi \in \Pi_{bc}(\mu(dx_{t+1:T} | x_{1:t}), \nu(dy_{t+1:T} | y_{1:t}))} \int \sum_{s=t+1}^T \varphi(s-t) c(x_s, y_s) \pi(dx_{t+1:T}, dy_{t+1:T} | x_{1:t}, y_{1:t}), \quad (2.5)$$

where $\varphi(\cdot)$ is a discounting function besides the power function. Note that the form (2.5) can be reformulated into (2.4) by redefining a new $\tilde{x}_t = (t, x_t)$. Since transitions of time are deterministic, the reformulation does not change the conditional probability kernels.

In Section 4.2.1, a concrete example is provided, demonstrating how time inconsistency emerges with nonlinear and state-dependent objectives.

2.2 Definition of equilibrium transport

To handle the time inconsistency and define a reasonable concept of “optimal” solutions, we should consider consistent plans that the agent can follow, instead of the pre-commitment solutions. The agent who is aware of time inconsistency should keep in mind that the objectives in the future are different. Inspired by the concept of subgame perfect Nash equilibrium, several works (Strotz, 1955; Björk and Murgoci, 2014; Björk et al., 2017) propose to reformulate the problem as a non-cooperative game between agents at time $t + 1, \dots, T - 1$ that are incarnations of the agent at time t , that is, a game between the current self and the future selves. An equilibrium solution, denoted as $\{\pi_t^*, \dots, \pi_{T-1}^*\}$ in a discrete-time setting, should satisfy the following property: If ourselves in the future time $t + 1, \dots, T - 1$ stick with $\{\pi_{t+1}^*, \dots, \pi_{T-1}^*\}$, then it is optimal for us at the current time t to adopt π_t^* . This backward recursive definition guarantees that the agent at each time t will not deviate from π_t^* .

Inspired by the above discussion, we define the equilibrium transport as follows. We refer to a transport plan π by its successive regular kernels $\{\bar{\pi}, \pi_1, \dots, \pi_{T-1}\}$ in (1.3). At time $t \in \{0, \dots, T-1\}$, denote a generic cost functional as $J(x_{1:t}, y_{1:t}; \pi)$, which implies that the current path is $(x_{1:t}, y_{1:t})$ and the agent uses the transport plan π in time $t, \dots, T - 1$.

Definition 2.1. Consider a given bicausal transport plan π^* with successive regular kernels $\{\bar{\pi}^*, \pi_1^*, \dots, \pi_{T-1}^*\}$.

1. For any $t = 1, \dots, T - 1$ and π^* -almost every path $(x_{1:t}, y_{1:t})$, consider any transport plan $\gamma \in \Pi(\mu(dx_{t+1}|x_{1:t}), \nu(dy_{t+1}|y_{1:t}))$. When $t = 0$, interpret $(x_{1:0}, y_{1:0})$ as none and consider $\bar{\gamma} \in \Pi(p_*^1 \mu, p_*^1 \nu)$.
2. Define a perturbed transport plan $\pi^{t,\gamma}$ as

$$\pi^{t,\gamma}(dx_{t+1:T}, dy_{t+1:T}|x_{1:t}, y_{1:t}) = \gamma(dx_{t+1}, dy_{t+1}|x_{1:t}, y_{1:t})\pi^*(dx_{t+2}, dy_{t+2}|x_{1:t+1}, y_{1:t+1})\dots \pi^*(dx_T, dy_T|x_{1:T-1}, y_{1:T-1}).$$

Then π^* is a subgame perfect Nash equilibrium bicausal transport plan if for every $t = 0, \dots, T - 1$ and π^* -almost every $(x_{1:t}, y_{1:t})$, we have

$$\inf_{\gamma \in \Pi(\mu(dx_{t+1}|x_{1:t}), \nu(dy_{t+1}|y_{1:t}))} J(x_{1:t}, y_{1:t}; \pi^{t,\gamma}) = J(x_{1:t}, y_{1:t}; \pi^{t,*}),$$

where

$$\pi^{t,*}(dx_{t+1:T}, dy_{t+1:T}|x_{1:t}, y_{1:t}) = \pi^*(dx_{t+1}, dy_{t+1}|x_{1:t}, y_{1:t})\pi^*(dx_{t+2}, dy_{t+2}|x_{1:t+1}, y_{1:t+1})\dots \pi^*(dx_T, dy_T|x_{1:T-1}, y_{1:T-1}).$$

We call π^* an equilibrium transport for simplicity. If π^* exists, define the equilibrium value function V as

$$V_t(x_{1:t}, y_{1:t}) = J(x_{1:t}, y_{1:t}; \pi^{t,*}).$$

2.3 The discrete case

To understand Definition 2.1 with an example, we revisit the regularized objective (2.3) and characterize an equilibrium transport as follows. If time moves to $t + 1$, the cost functional is given by

$$J(x_{1:t+1}, y_{1:t+1}; \pi) = \langle c(x_{1:T}, y_{1:T}), \pi(x_{t+2:T}, y_{t+2:T} | x_{1:t+1}, y_{1:t+1}) \rangle_F \\ + \left\langle f \left(\frac{\pi(x_{t+2:T}, y_{t+2:T} | x_{1:t+1}, y_{1:t+1})}{\mu(x_{t+2:T} | x_{1:t+1}) \otimes \nu(y_{t+2:T} | y_{1:t+1})} \right), \mu(x_{t+2:T} | x_{1:t+1}) \otimes \nu(y_{t+2:T} | y_{1:t+1}) \right\rangle_F.$$

If all agents at time $t + 1, \dots, T - 1$ adopt the equilibrium transport π^* , then

$$J(x_{1:t+1}, y_{1:t+1}; \pi^*) = V_{t+1}(x_{1:t+1}, y_{1:t+1}).$$

Next, we argue backwardly and consider the subproblem at time t with a perturbed transport plan $\pi^{t,\gamma} = \pi^*(x_{t+2:T}, y_{t+2:T} | x_{1:t+1}, y_{1:t+1})\gamma(x_{t+1}, y_{t+1})$. We have

$$J(x_{1:t}, y_{1:t}; \pi^{t,\gamma}) = \langle c(x_{1:T}, y_{1:T}), \pi^*(x_{t+2:T}, y_{t+2:T} | x_{1:t+1}, y_{1:t+1})\gamma(x_{t+1}, y_{t+1}) \rangle_F \\ + \left\langle f \left(\frac{\pi^*(x_{t+2:T}, y_{t+2:T} | x_{1:t+1}, y_{1:t+1})\gamma(x_{t+1}, y_{t+1})}{\mu(x_{t+1:T} | x_{1:t}) \otimes \nu(y_{t+1:T} | y_{1:t})} \right), \mu(x_{t+1:T} | x_{1:t}) \otimes \nu(y_{t+1:T} | y_{1:t}) \right\rangle_F.$$

Therefore, combining the two equations, we obtain the following recursive relationship between $J(x_{1:t}, y_{1:t}; \pi^{t,\gamma})$ and $J(x_{1:t+1}, y_{1:t+1}; \pi^*)$:

$$J(x_{1:t}, y_{1:t}; \pi^{t,\gamma}) = \langle J(x_{1:t+1}, y_{1:t+1}; \pi^*), \gamma(x_{t+1}, y_{t+1}) \rangle_F \\ - \left\langle f \left(\frac{\pi^*(x_{t+2:T}, y_{t+2:T} | x_{1:t+1}, y_{1:t+1})}{\mu(x_{t+2:T} | x_{1:t+1}) \otimes \nu(y_{t+2:T} | y_{1:t+1})} \right), \mu(x_{t+2:T} | x_{1:t+1}) \otimes \nu(y_{t+2:T} | y_{1:t+1}) \gamma(x_{t+1}, y_{t+1}) \right\rangle_F \\ + \left\langle f \left(\frac{\pi^*(x_{t+2:T}, y_{t+2:T} | x_{1:t+1}, y_{1:t+1})\gamma(x_{t+1}, y_{t+1})}{\mu(x_{t+1:T} | x_{1:t}) \otimes \nu(y_{t+1:T} | y_{1:t})} \right), \mu(x_{t+1:T} | x_{1:t}) \otimes \nu(y_{t+1:T} | y_{1:t}) \right\rangle_F.$$

By Definition 2.1, if all agents at time $t + 1, \dots, T - 1$ adopt the equilibrium transport $\{\pi_{t+1}^*, \dots, \pi_{T-1}^*\}$, then it is also optimal for the agent at time t to use π_t^* . Therefore, the recursive relationship should lead to the following equation for the value function:

$$V_t(x_{1:t}, y_{1:t}) = \inf_{\gamma \in \Pi(\mu(x_{t+1} | x_{1:t}), \nu(y_{t+1} | y_{1:t}))} \left[\langle V_{t+1}(x_{1:t+1}, y_{1:t+1}), \gamma(x_{t+1}, y_{t+1}) \rangle_F \right. \\ - \left\langle f \left(\frac{\pi^*(x_{t+2:T}, y_{t+2:T} | x_{1:t+1}, y_{1:t+1})}{\mu(x_{t+2:T} | x_{1:t+1}) \otimes \nu(y_{t+2:T} | y_{1:t+1})} \right), \mu(x_{t+2:T} | x_{1:t+1}) \otimes \nu(y_{t+2:T} | y_{1:t+1}) \gamma(x_{t+1}, y_{t+1}) \right\rangle_F \\ \left. + \left\langle f \left(\frac{\pi^*(x_{t+2:T}, y_{t+2:T} | x_{1:t+1}, y_{1:t+1})\gamma(x_{t+1}, y_{t+1})}{\mu(x_{t+1:T} | x_{1:t}) \otimes \nu(y_{t+1:T} | y_{1:t})} \right), \mu(x_{t+1:T} | x_{1:t}) \otimes \nu(y_{t+1:T} | y_{1:t}) \right\rangle_F \right].$$

Since the problem is finite and discrete, the infimum over γ is attained and leads to the conditional kernel π_t^* of an equilibrium transport. Moreover, there can be multiple equilibrium transport plans. The value function is continuous automatically under the discrete topology. We follow Björk and Murgoci (2014); Björk et al. (2017) and call the recursive relationship above of the value function V_t as the extended dynamic programming (DP) equation. For the discrete case with general nonlinear and state-dependent objectives, see Remark 4.7.

As a side remark, if we consider continuous measures μ and/or ν instead, the weak topology is not strong enough. Even convergence of probabilities under Wasserstein distance does not necessarily lead to convergence under f -divergence, including Jensen-Shannon, KL, reverse KL, total variation, and other divergences. See Arjovsky et al. (2017, Example 1). Since the continuity of value function is needed for the recursion, then we can only show the discrete case for the regularized objective (2.3) under the current weak topology.

3 The semi-discrete and Markovian case

In this section, we work with topological spaces without fixing any particular metrics. Theorem 3.3 and Corollary 3.5 provide the existence of equilibrium transport when \mathcal{X} is a finite discrete set with the discrete topology and \mathcal{Y} can be a general closed set in $\mathbb{R}^{T \times d}$. The current formulation is already computationally challenging. Indeed, Taşkesen et al. (2023, Theorem 2.2) showed that the computational complexity of the Wasserstein distance between a discrete probability measure supported on two points and the Lebesgue measure on the standard hypercube is already #P-hard.

Suppose the nonlinear and state-dependent objective is given by

$$\begin{aligned} J(x_t, y_t; \pi) &:= \int \sum_{k=t+1}^T c_k(x_t, y_t, x_k, y_k) \pi(dx_{t+1:T}, dy_{t+1:T} | x_t, y_t) \\ &\quad + G\left(x_t, y_t, \int h(x_T, y_T) \pi(dx_T, dy_T | x_t, y_t)\right). \end{aligned} \quad (3.1)$$

The function h only depends on (x_T, y_T) . The cost function c is separable and given by

$$c(w, v, x_{1:T}, y_{1:T}) := \sum_{k=1}^T c_k(w, v, x_k, y_k),$$

where w and v capture the state-dependence on x and y . The first two terms in $G(x_t, y_t, \cdot)$ are also state-dependent.

By convention, we interpret \mathcal{X}_0 and \mathcal{Y}_0 as singletons.

Assumption 3.1. (1) For each $t \in \{1, \dots, T\}$, \mathcal{X}_t is a non-empty finite discrete set equipped with the discrete topology $\mathcal{T}_{\mathcal{X}_t}$. \mathcal{X} is endowed with the product discrete topology.

(2) For each $k \in \{1, \dots, T\}$ and $i \in \{0, 1, \dots, T\}$, $c_k(x_i, y_i, x_k, y_k) : (\mathcal{X}_i \times \mathcal{Y}_i \times \mathcal{X}_k \times \mathcal{Y}_k, \mathcal{T}_{\mathcal{X}_i} \times \mathcal{T}_{\mathcal{Y}_i} \times \mathcal{T}_{\mathcal{X}_k} \times \mathcal{T}_{\mathcal{Y}_k}) \rightarrow (\mathbb{R}, \mathcal{T}_{\mathbb{R}})$ is continuous and bounded. Hence, when $i = k$, $c_k(x_k, y_k, x_k, y_k)$ is $\mathcal{T}_{\mathcal{X}_k} \times \mathcal{T}_{\mathcal{Y}_k}$ -continuous and bounded.

(3) $h(x_T, y_T) : (\mathcal{X}_T \times \mathcal{Y}_T, \mathcal{T}_{\mathcal{X}_T} \times \mathcal{T}_{\mathcal{Y}_T}) \rightarrow (\mathbb{R}, \mathcal{T}_{\mathbb{R}})$ is continuous and bounded.

(4) For each $t \in \{0, 1, \dots, T\}$, $G(x_t, y_t, g) : (\mathcal{X}_t \times \mathcal{Y}_t \times \mathbb{R}, \mathcal{T}_{\mathcal{X}_t} \times \mathcal{T}_{\mathcal{Y}_t} \times \mathcal{T}_{\mathbb{R}}) \rightarrow (\mathbb{R}, \mathcal{T}_{\mathbb{R}})$ is continuous and bounded.

Assumption 3.2. (1) The regular conditional kernels of μ and ν are Markovian and denoted as $\mu(dx_{t+1}|x_t)$ and $\nu(dy_{t+1}|y_t)$.

(2) $\nu(dy_{t+1}|y_t) : (\mathcal{Y}_t, \mathcal{T}_{\mathcal{Y}_t}) \rightarrow (\mathcal{P}(\mathcal{Y}_{t+1}), \mathcal{V}[C_b(\mathcal{Y}_{t+1}; \mathcal{T}_{\mathcal{Y}_{t+1}})])$ is Borel measurable.

With the discrete topology, we note that $\mu(dx_{t+1}|x_t)$ is continuous.

Under the current formulation, the extended DP equation is also Markovian:

$$\begin{aligned}
V_t(x_t, y_t) = \inf_{\gamma \in \Pi(\mu(dx_{t+1}|x_t), \nu(dy_{t+1}|y_t))} & \left[\int \left(c_{t+1}(x_t, y_t, x_{t+1}, y_{t+1}) + V_{t+1}(x_{t+1}, y_{t+1}) \right) \gamma(dx_{t+1}, dy_{t+1}) \right. \\
& - \int G(x_{t+1}, y_{t+1}, g_{t+1}(x_{t+1}, y_{t+1})) \gamma(dx_{t+1}, dy_{t+1}) \\
& + G\left(x_t, y_t, \int g_{t+1}(x_{t+1}, y_{t+1}) \gamma(dx_{t+1}, dy_{t+1})\right) \\
& - \int \sum_{k=t+2}^T b_k(x_{t+1}, y_{t+1}, x_{t+1}, y_{t+1}) \gamma(dx_{t+1}, dy_{t+1}) \\
& \left. + \int \sum_{k=t+2}^T b_k(x_t, y_t, x_{t+1}, y_{t+1}) \gamma(dx_{t+1}, dy_{t+1}) \right]. \tag{3.2}
\end{aligned}$$

In this equation,

- (a) the boundary condition for V is

$$V_T(x_T, y_T) = G(x_T, y_T, h(x_T, y_T));$$

- (b) denote an optimizer for the equation (3.2) at time t as $\pi^*(dx_{t+1}, dy_{t+1}|x_t, y_t)$. Concatenate these kernels to obtain

$$\pi^*(dx_{t+1:T}, dy_{t+1:T}|x_t, y_t) = \pi^*(dx_{t+1}, dy_{t+1}|x_t, y_t) \dots \pi^*(dx_T, dy_T|x_{T-1}, y_{T-1}); \tag{3.3}$$

- (c) the function sequences g_{t+1} and b_k in (3.2) are given by

$$\begin{aligned}
g_{t+1}(x_{t+1}, y_{t+1}) &:= \int h(x_T, y_T) \pi^*(dx_T, dy_T|x_{t+1}, y_{t+1}), \\
b_k(w, v, x_{t+1}, y_{t+1}) &:= \int c_k(w, v, x_k, y_k) \pi^*(dx_k, dy_k|x_{t+1}, y_{t+1}),
\end{aligned}$$

with $\pi^*(dx_k, dy_k|x_{t+1}, y_{t+1})$ obtained backwardly using (3.3). For a given t , the index $k \in \{t+2, \dots, T\}$ and the state-dependent terms $w \in \mathcal{X}_i$ and $v \in \mathcal{Y}_i$, with $i \in \{0, \dots, t+1\}$.

The proof of Theorem 3.3 is given in Section A.1 of the e-companion. The main idea is the Borel measurable selection theorem (Brown and Purves, 1973) with a careful treatment of the Polish topology (Kechris, 2012, Theorem 13.11). Moreover, the proof shows that there is a finer Polish topology such that $\pi^*(dx_{t+1}, dy_{t+1}|x_t, y_t)$ and $V_t(x_t, y_t)$ are continuous.

Theorem 3.3. *Suppose Assumptions 3.1 and 3.2 hold. Then there exists a Borel measurable optimizer $\pi^*(dx_{t+1}, dy_{t+1}|x_t, y_t)$ for (3.2). Moreover, π^* defined recursively by (3.3) is an equilibrium bicausal transport plan in the sense of Definition 2.1. The value function $V_t(x_t, y_t)$ in (3.2) is Borel measurable.*

Note that

$$V_{t+1}(x_{t+1}, y_{t+1}) = \sum_{k=t+2}^T b_k(x_{t+1}, y_{t+1}, x_{t+1}, y_{t+1}) + G(x_{t+1}, y_{t+1}, g_{t+1}(x_{t+1}, y_{t+1})).$$

Then the extended DP equation (3.2) reduces to

$$V_t(x_t, y_t) = \inf_{\gamma \in \Pi(\mu(dx_{t+1}|x_t), \nu(dy_{t+1}|y_t))} \left[\int c_{t+1}(x_t, y_t, x_{t+1}, y_{t+1}) \gamma(dx_{t+1}, dy_{t+1}) \right. \\ \left. + G\left(x_t, y_t, \int g_{t+1}(x_{t+1}, y_{t+1}) \gamma(dx_{t+1}, dy_{t+1})\right) \right. \\ \left. + \int \sum_{k=t+2}^T b_k(x_t, y_t, x_{t+1}, y_{t+1}) \gamma(dx_{t+1}, dy_{t+1}) \right]. \quad (3.4)$$

Based on this observation, we consider the lower semicontinuous (l.s.c.) costs bounded from below.

Assumption 3.4. (1) *Assumption 3.1 (1) holds.*

(2) *For each $k \in \{1, \dots, T\}$ and $i \in \{0, 1, \dots, T\}$, $c_k(x_i, y_i, x_k, y_k) : (\mathcal{X}_i \times \mathcal{Y}_i \times \mathcal{X}_k \times \mathcal{Y}_k, \mathcal{T}_{\mathcal{X}_i} \times \mathcal{T}_{\mathcal{Y}_i} \times \mathcal{T}_{\mathcal{X}_k} \times \mathcal{T}_{\mathcal{Y}_k}) \rightarrow (\mathbb{R}, \mathcal{T}_{\mathbb{R}})$ is l.s.c. and bounded from below. Hence, when $i = k$, $c_k(x_k, y_k, x_k, y_k)$ is $\mathcal{T}_{\mathcal{X}_k} \times \mathcal{T}_{\mathcal{Y}_k}$ -l.s.c. and bounded from below.*

(3) *$h(x_T, y_T) : (\mathcal{X}_T \times \mathcal{Y}_T, \mathcal{T}_{\mathcal{X}_T} \times \mathcal{T}_{\mathcal{Y}_T}) \rightarrow (\mathbb{R}, \mathcal{T}_{\mathbb{R}})$ is l.s.c. and bounded from below.*

(4) *For each $t \in \{0, 1, \dots, T\}$, $G(x_t, y_t, g) : (\mathcal{X}_t \times \mathcal{Y}_t \times \mathbb{R}, \mathcal{T}_{\mathcal{X}_t} \times \mathcal{T}_{\mathcal{Y}_t} \times \mathcal{T}_{\mathbb{R}}) \rightarrow (\mathbb{R}, \mathcal{T}_{\mathbb{R}})$ is l.s.c. and $G(x_t, y_t, \cdot)$ is nondecreasing for each (x_t, y_t) .*

Corollary 3.5 extends Theorem 3.3 to l.s.c. costs. In the proof, we actually show that there is a finer Polish topology such that $\pi^*(dx_{t+1}, dy_{t+1}|x_t, y_t)$ is continuous and $V_t(x_t, y_t)$ is l.s.c.

Corollary 3.5. *Suppose Assumptions 3.2 and 3.4 hold. Then there exists a Borel measurable optimizer $\pi^*(dx_{t+1}, dy_{t+1}|x_t, y_t)$ for (3.2) or equivalently (3.4). Moreover, π^* defined recursively by (3.3) is an equilibrium bicausal transport plan in the sense of Definition 2.1. The value function $V_t(x_t, y_t)$ in (3.2) is Borel measurable.*

4 Continuous and non-Markovian cases with parametric couplings

4.1 Metric spaces and Wasserstein distances

For generic probability measures and unbounded cost functions, metric spaces are needed for growth rate conditions. Consider \mathcal{X} and \mathcal{Y} with the Euclidean topology. Given a fixed $p \in [1, \infty)$, introduce the metric as $d_{\mathcal{X}}(x_{1:T}, x'_{1:T}) = \left[\sum_{t=1}^T d_{\mathcal{X}_t}(x_t, x'_t)^p \right]^{1/p}$ for $x, x' \in \mathcal{X}$, where $d_{\mathcal{X}_t}(x_t, x'_t) := |x_t - x'_t|$. The Wasserstein space of order p is given by

$$\mathcal{P}_p(\mathcal{X}) := \left\{ \mu \in \mathcal{P}(\mathcal{X}) \mid \int_{\mathcal{X}} d_{\mathcal{X}}(x_{1:T}, \bar{x}_{1:T})^p \mu(dx) < \infty \right\}$$

for some fixed $\bar{x}_{1:T} \in \mathcal{X}$. We always equip $\mathcal{P}_p(\mathcal{X})$ with the Wasserstein distance of order p :

$$W_p(\mu, \mu') = \left(\inf_{\gamma \in \Pi(\mu, \mu')} \int_{\mathcal{X} \times \mathcal{X}} d_{\mathcal{X}}(x, x')^p \gamma(dx, dx') \right)^{1/p}. \quad (4.1)$$

Let

$$C_p(\mathcal{X}) := \left\{ f \in C(\mathcal{X}) \mid \exists \text{ constant } C > 0, |f(x)| \leq C(1 + d_{\mathcal{X}}(x, \bar{x})^p) \right\}$$

be the set of continuous functions from \mathcal{X} to \mathbb{R} with a growth rate of order p in $d_{\mathcal{X}}(x, \bar{x})$. Consider a sequence of probability measures $\{\mu^k\}_{k \in \mathbb{N}}$ in $\mathcal{P}_p(\mathcal{X})$ and μ as another probability measure in $\mathcal{P}_p(\mathcal{X})$. Recall that μ^k converges weakly in $\mathcal{P}_p(\mathcal{X})$ to μ means that μ^k converges to μ in the usual weak convergence and $\int d_{\mathcal{X}}(x, \bar{x})^p \mu^k(dx) \rightarrow \int d_{\mathcal{X}}(x, \bar{x})^p \mu(dx)$; see Villani (2009, Definition 6.7). By Villani (2009, Theorem 6.8), $W_p(\mu^k, \mu) \rightarrow 0$ is equivalent to μ^k converges weakly in $\mathcal{P}_p(\mathcal{X})$ to μ .

Similarly, we can replace $(\mathcal{X}, d_{\mathcal{X}})$ with any metric space $(\mathcal{S}, d_{\mathcal{S}})$ that is Polish and define $\mathcal{P}_p(\mathcal{S})$ and $C_p(\mathcal{S})$ accordingly. In particular, we denote the metric for $\mathcal{X} \times \mathcal{Y}$ as

$$d((x, y), (\bar{x}, \bar{y})) = [d_{\mathcal{X}}(x, \bar{x})^p + d_{\mathcal{Y}}(y, \bar{y})^p]^{1/p}.$$

4.2 Parametric couplings

For each time $t \in \{0, \dots, T-1\}$, we use $\gamma(dx_{t+1}, dy_{t+1} | \theta_{t+1})$ to model elements in a subset of $\mathcal{P}_p(\mathcal{X}_{t+1} \times \mathcal{Y}_{t+1})$. Suppose the parameter θ_{t+1} is in a Polish topological vector space $(\Theta_{t+1}, \mathcal{T}_{\Theta_{t+1}})$ with a complete compatible metric $d_{\Theta_{t+1}}$. The parametric model γ may not enumerate every element in $\mathcal{P}_p(\mathcal{X}_{t+1} \times \mathcal{Y}_{t+1})$ and can be regarded as a form of dimension reduction. For example, the agent may want to narrow down the candidate couplings and consider specific parametric distributions only. The dual potential functions are commonly modeled by neural networks, which provide a parametric form for the couplings if regularization is also considered; see Seguy et al. (2018, Equation (8)). Another method in Delon and Desolneux (2020) restricts to Gaussian mixtures models as the couplings. Parametric methods can reduce the computational burden while sacrifice the accuracy. If we take $\Theta_{t+1} = \mathcal{P}_p(\mathcal{X}_{t+1} \times \mathcal{Y}_{t+1})$, it collapses to the classical formulation. We term the parametric kernel as the parametric transport (coupling) and the concatenation is denoted as

$$\gamma(dx_{t+1:T}, dy_{t+1:T} | \theta_{t+1:T}) := \gamma(dx_T, dy_T | \theta_T) \dots \gamma(dx_{t+1}, dy_{t+1} | \theta_{t+1}). \quad (4.2)$$

Consider a general nonlinear and state-dependent objective which is not necessarily separable:

$$\begin{aligned} J(x_{1:t}, y_{1:t}; \theta_{t+1:T}) &:= \int c(x_t, y_t, x_{1:T}, y_{1:T}) \gamma(dx_{t+1:T}, dy_{t+1:T} | \theta_{t+1:T}) \\ &\quad + G\left(x_t, y_t, \int h(x_{1:T}, y_{1:T}) \gamma(dx_{t+1:T}, dy_{t+1:T} | \theta_{t+1:T})\right). \end{aligned} \quad (4.3)$$

The minimization is over $\theta_{t+1:T}$, which should satisfy the bicausal constraints

$$\gamma(dx_{t+1:T}, dy_{t+1:T} | \theta_{t+1:T}) \in \Pi_{bc}(\mu(dx_{t+1:T} | x_{1:t}), \nu(dy_{t+1:T} | y_{1:t})).$$

We impose the following assumptions on the objective and probability measures.

Assumption 4.1. (1) For each $t = 0, 1, \dots, T$, $c(x_t, y_t, x_{1:T}, y_{1:T}) \in C_p(\mathcal{X}_{1:T} \times \mathcal{Y}_{1:T})$.

(2) $h(\cdot, \cdot)$ is continuous and

$$|h(x_{1:T}, y_{1:T})| \leq C(1 + d((x_{1:T}, y_{1:T}), (\bar{x}_{1:T}, \bar{y}_{1:T}))^{1/r})$$

for some constant $r > 0$ satisfying $1/r \leq p$.

(3) For each $t = 0, 1, \dots, T$, $G(x_t, y_t, g) : (\mathcal{X}_t \times \mathcal{Y}_t \times \mathbb{R}, \mathcal{T}_{\mathcal{X}_t} \times \mathcal{T}_{\mathcal{Y}_t} \times \mathcal{T}_{\mathbb{R}}) \rightarrow (\mathbb{R}, \mathcal{T}_{\mathbb{R}})$ is continuous and $|G(x_t, y_t, g)| \leq C[1 + |g|^{pr} + d((x_t, y_t), (\bar{x}_t, \bar{y}_t))^p]$.

Assumption 4.2. (1) $x_{1:t} \mapsto \mu(dx_{t+1:T} | x_{1:t})$ is continuous with respect to metric $d_{\mathcal{X}}$ on the domain $\mathcal{X}_{1:t}$ and the W_p metric on the range $\mathcal{P}_p(\mathcal{X}_{1:t})$.

(2) For constant $a \in \{1/r, p\}$,

$$\int_{\mathcal{X}_{t+1:T}} d\mathcal{X}(x_{1:T}, \bar{x}_{1:T})^a \mu(dx_{t+1:T}|x_{1:t}) \leq C[1 + d\mathcal{X}(x_{1:t}, \bar{x}_{1:t})^a].$$

Same assumptions on ν hold with the metric d_Y .

Assumption 4.2(2) is used in (A.5) for the growth rate.

Introduce the correspondence $D_t : \mathcal{X}_{1:t} \times \mathcal{Y}_{1:t} \rightarrow \Theta_{t+1}$ as

$$(x_{1:t}, y_{1:t}) \mapsto \{\theta_{t+1} \in \Theta_{t+1} | \gamma(dx_{t+1}, dy_{t+1} | \theta_{t+1}) \in \Pi(\mu(dx_{t+1} | x_{1:t}), \nu(dy_{t+1} | y_{1:t}))\}. \quad (4.4)$$

We use a notation \rightarrow to highlight that the correspondence maps a point to a subset.

The equilibrium parametric transport is characterized with:

$$V_t(x_{1:t}, y_{1:t}) = \inf_{\theta_{t+1} \in D_t(x_{1:t}, y_{1:t})} f(x_{1:t}, y_{1:t}, \theta_{t+1}), \quad (4.5)$$

where

$$\begin{aligned} f(x_{1:t}, y_{1:t}, \theta_{t+1}) := & G\left(x_t, y_t, \int g_{t+1}(x_{1:t+1}, y_{1:t+1}) \gamma(dx_{t+1}, dy_{t+1} | \theta_{t+1})\right) \\ & + \int b_{t+1}(x_t, y_t, x_{1:t+1}, y_{1:t+1}) \gamma(dx_{t+1}, dy_{t+1} | \theta_{t+1}). \end{aligned} \quad (4.6)$$

In this equation,

(a) the boundary condition for V is

$$V_T(x_{1:T}, y_{1:T}) = c(x_T, y_T, x_{1:T}, y_{1:T}) + G(x_T, y_T, h(x_{1:T}, y_{1:T}));$$

(b) denote an optimizer for the equation (4.5) at time t as $\theta_{t+1}^*(x_{1:t}, y_{1:t})$. It yields the equilibrium parametric kernels in the sense of Definition 2.1 when kernels are restricted in the parametric spaces:

$$\begin{aligned} & \gamma(dx_{t+1:T}, dy_{t+1:T} | \theta_{t+1:T}^*(x_{1:t}, y_{1:t})) \\ & := \gamma(dx_T, dy_T | \theta_T^*(x_{1:T-1}, y_{1:T-1})) \dots \gamma(dx_{t+1}, dy_{t+1} | \theta_{t+1}^*(x_{1:t}, y_{1:t})); \end{aligned} \quad (4.7)$$

(c) the function sequences g_{t+1} and b_{t+1} in (4.5) are given by

$$\begin{aligned} g_{t+1}(x_{1:t+1}, y_{1:t+1}) &:= \int h(x_{1:T}, y_{1:T}) \gamma(dx_{t+2:T}, dy_{t+2:T} | \theta_{t+2:T}^*(x_{1:t+1}, y_{1:t+1})), \\ b_{t+1}(w, v, x_{1:t+1}, y_{1:t+1}) &:= \int c(w, v, x_{1:T}, y_{1:T}) \gamma(dx_{t+2:T}, dy_{t+2:T} | \theta_{t+2:T}^*(x_{1:t+1}, y_{1:t+1})), \end{aligned}$$

with $\gamma(dx_{t+2:T}, dy_{t+2:T} | \theta_{t+2:T}^*(x_{1:t+1}, y_{1:t+1}))$ in (4.7) and $\theta_{i+1}^*(x_{1:i}, y_{1:i})$, $i = t+1, \dots, T-1$, are obtained backwardly using (4.5).

Recall that a function $f : \mathcal{S} \rightarrow \mathbb{R}$ defined on a convex subset \mathcal{S} of a real vector space is quasiconvex if for all $s, s' \in \mathcal{S}$ and $\lambda \in [0, 1]$, we have $f(\lambda s + (1 - \lambda)s') \leq \max\{f(s), f(s')\}$. If furthermore $f(\lambda s + (1 - \lambda)s') < \max\{f(s), f(s')\}$ for all $s \neq s'$ and $\lambda \in (0, 1)$, then f is strictly quasiconvex. Every convex function is quasiconvex. Besides, please refer to Charalambos and Aliprantis (2013, Definition 17.2) for the definition of lower and upper hemicontinuity.

Assumption 4.3. For each $t \in \{0, \dots, T-1\}$,

- (1) $\gamma(dx_{t+1}, dy_{t+1}|\theta_{t+1}) : (\Theta_{t+1}, d_{\Theta_{t+1}}) \rightarrow \mathcal{P}_p(\mathcal{X}_{t+1} \times \mathcal{Y}_{t+1})$ is continuous;
- (2) D_t in (4.4) is a continuous correspondence with non-empty, convex, and compact images, under the product topology $\mathcal{T}_{\mathcal{X}_{1:t}} \times \mathcal{T}_{\mathcal{Y}_{1:t}} \times \mathcal{T}_{\Theta_{t+1}}$;
- (3) given an arbitrary path $(x_{1:t}, y_{1:t}) \in \mathcal{X}_{1:t} \times \mathcal{Y}_{1:t}$, suppose $f(x_{1:t}, y_{1:t}, \theta_{t+1})$ in (4.6) is strictly quasiconvex in $\theta_{t+1} \in \Theta_{t+1}$.

We apply a version of Berge's maximum theorem with strict quasiconcavity, see Sundaram (1996, Theorem 9.14 and Corollary 9.20) or Charalambos and Aliprantis (2013, Theorem 17.31), to prove the existence and uniqueness of the equilibrium parametric transport. The proof is given in Section A.2.

Theorem 4.4. Suppose Assumptions 4.1, 4.2, and 4.3 hold. Then

- (a) there is a continuous and unique optimizer, $\theta_{t+1}^*(x_{1:t}, y_{1:t}) : (\mathcal{X}_{1:t} \times \mathcal{Y}_{1:t}, d) \rightarrow (\Theta_{t+1}, d_{\Theta_{t+1}})$, for the extended DP equation (4.5);
- (b) the equilibrium parametric kernel

$$\gamma(dx_{t+1:T}, dy_{t+1:T}|\theta_{t+1:T}^*(x_{1:t}, y_{1:t})) : (\mathcal{X}_{1:t} \times \mathcal{Y}_{1:t}, d) \rightarrow \mathcal{P}_p(\mathcal{X}_{t+1:T} \times \mathcal{Y}_{t+1:T})$$

in (4.7), is continuous and unique;

- (c) the corresponding value function V_t satisfies (4.5) and $V_t \in C_p(\mathcal{X}_{1:t} \times \mathcal{Y}_{1:t})$.

Remark 4.5. If the objective $f(x_{1:t}, y_{1:t}, \theta_{t+1})$ does not satisfy the strict quasiconvexity in Assumption 4.3 (3), we could also include a regularization term on θ_{t+1} directly, such as $|\theta_{t+1}|^2$. If the regularization term is $\mathcal{T}_{\Theta_{t+1}}$ -continuous, then it can be treated similarly by Theorem 4.4.

It is direct to recover the classical formulation by setting $\Theta_{t+1} = \mathcal{P}_p(\mathcal{X}_{t+1} \times \mathcal{Y}_{t+1})$, $t \in \{0, \dots, T-1\}$.

Corollary 4.6. Suppose

- (1) Assumptions 4.1 and 4.2 hold;
- (2) $\Theta_{t+1} = \mathcal{P}_p(\mathcal{X}_{t+1} \times \mathcal{Y}_{t+1})$, $t \in \{0, \dots, T-1\}$;
- (3) for each given $t = 0, 1, \dots, T-1$ and an arbitrary path $(x_{1:t}, y_{1:t}) \in \mathcal{X}_{1:t} \times \mathcal{Y}_{1:t}$, suppose $f(x_{1:t}, y_{1:t}, \gamma)$ in (4.6) is strictly quasiconvex in any

$$\gamma(dx_{t+1}, dy_{t+1}) \in \Pi(\mu(dx_{t+1}|x_{1:t}), \nu(dy_{t+1}|y_{1:t})).$$

Then

- (a) there is a continuous and unique optimizer, $\pi^*(dx_{t+1}, dy_{t+1}|x_{1:t}, y_{1:t}) : (\mathcal{X}_{1:t} \times \mathcal{Y}_{1:t}, d) \rightarrow \mathcal{P}_p(\mathcal{X}_{t+1} \times \mathcal{Y}_{t+1})$, for the extended DP equation (4.5);
- (b) the equilibrium transport $\pi^*(dx_{t+1:T}, dy_{t+1:T}|x_{1:t}, y_{1:t}) : (\mathcal{X}_{1:t} \times \mathcal{Y}_{1:t}, d) \rightarrow \mathcal{P}_p(\mathcal{X}_{t+1:T} \times \mathcal{Y}_{t+1:T})$ in (4.7), is continuous and unique;
- (c) the corresponding value function V_t satisfies (4.5) and $V_t \in C_p(\mathcal{X}_{1:t} \times \mathcal{Y}_{1:t})$.

Remark 4.7. *For the special case that μ and ν are discrete measures with finite supports, the extended DPP is straightforward. When \mathcal{X} and \mathcal{Y} are equipped with discrete topology, the value function and the correspondence are continuous automatically. There exists an equilibrium bicausal transport plan π^* which may not be unique. The strict quasiconvexity is not needed for the existence. However, we can regard probability masses as parameters and obtain the uniqueness if strict quasiconvexity holds.*

4.2.1 Example: Gaussian data

It is rare for continuous OT problems to have explicit solutions, even in the single-period case. One exception is the Gaussian distribution. As an explicit example illustrating Theorem 4.4, we consider μ and ν as Gaussian distributions with linear dynamics:

$$\begin{aligned} x_{t+1} &= x_t + \lambda_t, & \lambda_t &\sim N(0, 1), \\ y_{t+1} &= y_t + \eta_t, & \eta_t &\sim N(0, 1). \end{aligned}$$

For simplicity, suppose $x_t \in \mathbb{R}$ and $y_t \in \mathbb{R}$ are one-dimensional. The white Gaussian noise process $\{\lambda_t\}$ follow the standard normal distribution and are independent of each other. Impose the same condition on $\{\eta_t\}$.

Consider a two-period problem with a nonlinear and state-dependent objective:

$$\left(x_0 y_0 - \int x_2 y_2 \pi(dx_2, dy_2 | x_0, y_0) \right)^2. \quad (4.8)$$

The initial states x_0 and y_0 are fixed as constants.

We assume that the agent considers only normal distribution as couplings. At time $t = 1$, the agent seeks an optimal coupling which is a bivariate normal distribution $\gamma(dx_2, dy_2 | \theta_2)$ with marginals $x_2 \sim N(x_1, 1)$ and $y_2 \sim N(y_1, 1)$ and $\theta_2 \in [-1, 1]$ as the correlation between x_2 and y_2 . Since the first term in the square is state-dependent, the objective at time 1 is

$$\left(x_1 y_1 - \int x_2 y_2 \gamma(dx_2, dy_2 | \theta_2) \right)^2.$$

Then $f(x_1, y_1, \theta_2) = (x_1 y_1 - \theta_2 \times 1 \times 1 - x_1 y_1)^2 = \theta_2^2$, which is strictly quasiconvex in $\theta_2 \in [-1, 1]$. For other conditions in Assumptions 4.1, 4.2, and 4.3, we take $1/r = 2$ and $p = 4$ as the growth rate. Assumptions 4.1 and 4.2 are satisfied. $\gamma(dx_2, dy_2 | \theta_2)$ is continuous in θ_2 with the type-4 Wasserstein metric, by properties of the normal distribution and Villani (2009, Theorem 6.8). Clearly, the correspondence $D_1 : (x_1, y_1) \rightarrow [-1, 1]$ satisfies Assumption 4.3 (2). Theorem 4.4 shows that $\theta_2^*(x_1, y_1) = 0$ is the unique optimizer at time 1. Similarly, $\theta_1^*(x_0, y_0) = 0$, which is also unique. In this case, the restriction on normal couplings is not too restrictive since it gives a value function equal to zero.

Consider the agent who ignores time inconsistency and minimizes the objective (4.8) at time 0 only. Any constant (θ_1, θ_2) with $\theta_2 + \theta_1 = 0$ is an optimizer for $(x_0 y_0 - \int x_2 y_2 \pi(dx_2, dy_2 | x_0, y_0))^2 = (\theta_2 + \theta_1)^2$. However, for nonzero θ_1 , the agent at time 1 will find that it is optimal to deviate from $\theta_2 = -\theta_1$. Therefore, it is possible to have a unique equilibrium parametric transport but multiple globally optimal parametric transports.

5 A job market model with inertia

5.1 Matching as an optimal transport problem

To motivate our equilibrium transport job market model, we first review the connection between a CEO compensation model in Gabaix and Landier (2008) and the classical OT problem, following Galichon (2016, Chapter 4).

Gabaix and Landier (2008) considered a matching problem between firms and potential managers. Consider the static setting with $T = 1$ for simplicity. Assume there are the same number of managers and firms, represented by scalar rank characteristics $x \sim \mu$ and $y \sim \nu$, respectively. The manager of type x can generate earnings of $\Phi(x, y)$ for the firm of type y . Suppose the manager of type x receives a salary of $\psi(x)$. The firm y chooses the optimal manager that maximizes the earnings after deducting the wage:

$$\sup_{x \in \mathcal{X}} \Phi(x, y) - \psi(x). \quad (5.1)$$

Denote the optimal value in (5.1) as $\phi(y)$ for each $y \in \mathcal{Y}$. The pair (ψ, ϕ) is a solution to the following problem:

$$\inf_{\psi(x) + \phi(y) \geq \Phi(x, y)} \int_{\mathcal{X}} \psi(x) \mu(dx) + \int_{\mathcal{Y}} \phi(y) \nu(dy). \quad (5.2)$$

The Kantorovich duality shows that (5.2) is the dual for the primal problem:

$$\sup_{\pi \in \Pi(\mu, \nu)} \int_{\mathcal{X} \times \mathcal{Y}} \Phi(x, y) \pi(dx, dy). \quad (5.3)$$

It gives a clear connection between the CEO compensation problem in Gabaix and Landier (2008) and the OT problem. Gabaix and Landier (2008) aims to determine the function $\psi(x)$ for salaries. A crucial assumption in Gabaix and Landier (2008) is that, the total earnings are higher when the *positive assortative matching* (PAM) is adopted, that is, managers of higher types are matched with firms of higher types and the lower types with the lower types. Formally, it means that if $\bar{x} \geq \underline{x}$ and $\bar{y} \geq \underline{y}$, then $\Phi(\bar{x}, \bar{y}) + \Phi(\underline{x}, \underline{y}) \geq \Phi(\bar{x}, \underline{y}) + \Phi(\underline{x}, \bar{y})$. This property is called supermodular (Galichon, 2016, Section 4.2, Equation (4.7)). Examples include the Cobb-Douglas function $x^a y^b$, $a, b > 0$ and $-|x - y|^p$, $p \geq 1$. Importantly, if $\Phi(x, y)$ is supermodular, then the optimal coupling is the PAM (Galichon, 2016, Theorem 4.3).

Gabaix and Landier (2008) interpreted x and y as manager talents and firm sizes. An insight they found is that a bigger firm should hire a more talented manager and pay a higher salary.

5.2 The strengths and weaknesses of positive assortative matching

We can compare this theoretical conclusion in Gabaix and Landier (2008) with the empirical data. Indeed, Roberts' law (Gabaix and Landier, 2008) states that CEO compensation is roughly proportional to (firm size) $^\kappa$, with a typical empirical exponent $\kappa \simeq 1/3$.

Nevertheless, empirical data from executive job markets do not always show a perfect employer-employee correspondence. Figure 1 plots the wages and net sales data for the Industrials sector in the fiscal year of 2021. A power-law relationship holds approximately, but some big firms deviate from the Roberts' law and underpay their managers. Another specific example is that Nvidia has both larger market values and annual net sales than its competitor AMD. However, the average annual compensation of Nvidia's CEO, Jen-Hsun Huang, is significantly lower than that of AMD's CEO, Lisa Su, who earned a total of \$55.763 million more than Huang over a ten-year period. The

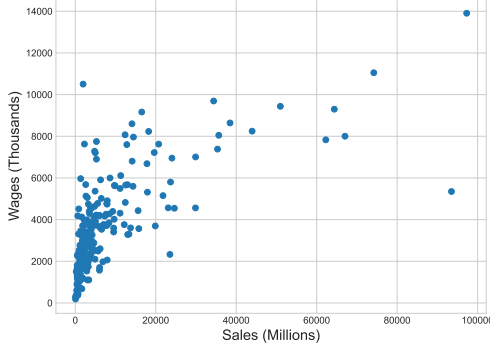


Figure 1: Sale-wage relationship in the Industrials sector in the fiscal year of 2021.

last but not least example is Warren Buffett, whose average annual compensation from 2012 to 2021 was only \$395,450.

These empirical observations reveal that the supermodular surplus function $\Phi(x, y)$ requires adjustments, which motivates our formulation in a dynamic setting.

5.3 Matching with a state-dependent preference

Consider a time horizon of T years, where we observe a time series of employer characteristics $(x_1, \dots, x_t, \dots, x_T) \sim \mu$. If employers prioritize profitability, we use the net sale ranks of employers as x . Sales data tend to be more stable than stock market values. If employers are universities, then rankings are readily available. For employees, commonly used characteristics include talent and salary, while talent is not observable. In this paper, we use the ranks of salaries as the characteristics of employees and denote ν as the distribution of salary ranks.

In the multi-period matching, bicausality is a natural requirement, meaning that no future information can be utilized. Both employers and employees are in symmetric positions when choosing each other. If the PAM holds perfectly, then the optimal employer-employee matching should assign the employer ranked number n with the employee ranked number n . Denote x_t as the rank of employers and y_t as the rank of employees at time t . The ranks x_t and y_t have the same range since the numbers of employers and employees are equal. With a discount factor $\delta \in [0, 1]$, a multi-period model that yields the PAM is

$$\inf_{\pi \in \Pi_{bc}(\mu, \nu)} \int \sum_{t=1}^T \delta^t |x_t - y_t| \pi(dx_{1:T}, dy_{1:T}). \quad (5.4)$$

To be consistent with our previous formulations (3.1) and (4.6), we consider minimization instead of maximization as in (5.3). In contrast to the Cobb-Douglas function, the absolute value $|x - y|$ does not involve any hyperparameters.

As mentioned above, some high-ranked firms pay less to executives and some industries are less consistent with the Roberts' law. We conjecture that there are incentives to maintain the original matching, regardless of its efficiency. For example, there may be implicit benefits to continuing to work for the same company, particularly if an employee is the founder. Additionally, employers may want to preserve the previous ranking of wages among their peers. We attempt to quantify this conjecture and refine the benchmark model (5.4) using the equilibrium transport method. For any time $t > 1$, we introduce a new term to reduce the cost if we keep similar matching and modify

the objective (5.4) to

$$\inf_{\pi \in \Pi_{bc}(\mu^t, \nu^t)} \int \left[-\alpha e^{-\frac{|x_{t+1}-x_t|+|y_{t+1}-y_t|}{\tau}} + \sum_{s=t+1}^T \delta^s |x_s - y_s| \right] \pi(dx_{t+1:T}, dy_{t+1:T} | x_{1:t}, y_{1:t}). \quad (5.5)$$

$\Pi_{bc}(\mu^t, \nu^t)$ uses simplified notations $\mu^t = \mu(dx_{t+1:T} | x_{1:t})$ and $\nu^t = \nu(dy_{t+1:T} | y_{1:t})$. α is a constant to be determined and $\tau > 0$ is a scaling constant. We call the first term the state-dependent preference function. We consider an exponential function for a fast decay when (x_{t+1}, y_{t+1}) deviates from the previous (x_t, y_t) . If we interpret $0/0 = 0$ and set $\tau = 0$, the state-dependent function also includes the indicator function $\mathbf{1}_{\{x_{t+1}=x_t, y_{t+1}=y_t\}}$ as a special case. The motivation for the state-dependent term can be further explained as follows:

1. Federal securities laws require disclosure of compensation paid to high-ranking executives of public companies. These companies are typically required to provide a Summary Compensation Table with executive compensation for the past *three* fiscal years ^[1] in their annual financial statement files (usually annual proxy statements). This requirement is intended to help stakeholders better understand year-over-year changes in compensation. As such, the state-dependent term reflects the concerns and practices of stakeholders and regulators.
2. Commonly, the current firm-wage matching depends on previous ones for financial reasons. For example, executive compensation programs in public companies often have several components, such as an annual base salary, an annual cash incentive, and long-term equity awards. The base salary tends to remain stable over time, while cash incentives and long-term equity awards are often linked to financial performance, such as annual sales, revenues, and market values. These factors can exhibit momentum and depend on past performance. Our state-dependent term captures this potential dependence on the previous firm-wage matching.
3. From a psychological and behavioral perspective, this specification also aligns with the *status quo bias* if $\alpha > 0$. People prefer to keep their current state. The employer may maintain a similar compensation rank among peers in the same industry. The employee may not resign and find a new job even if he/she is underpaid, possibly due to the status quo bias and relocation costs.

Overall, the state-dependent term with $\alpha > 0$ is a form of persistence or inertia to favor matching pairs close to the previous pair (x_t, y_t) . In contrast, the PAM favors pairs with $x_{t+1} = y_{t+1}$ regardless of previous states.

The problem (5.5) becomes state-dependent and thus is time-inconsistent. Since we consider x and y as ranks, the extended DP equation in the discrete case is sufficient. Denoting the equilibrium transport plan for a given α as $\pi(\alpha)$, we can calculate the classical Wasserstein distance $\mathcal{W}(\pi(\alpha), \pi_r)$ between $\pi(\alpha)$ and the real transport plan π_r :

$$\mathcal{W}(\pi(\alpha), \pi_r) := \inf_{\gamma \in \Pi(\pi(\alpha), \pi_r)} \int (|x_t - x'_t| + |y_t - y'_t|) d\gamma. \quad (5.6)$$

By varying α , we can find α minimizing $\mathcal{W}(\pi(\alpha), \pi_r)$. When the optimal α is negative, it indicates that the data prefer to deviate from the previous matching, while a positive value of α indicates that the data tend to maintain the previous matching.

In the next two sections, we investigate the inertia, measured by state dependence, of two job markets: top-ranking executives and academia (faculty and postdocs). The choice of these markets is mainly due to the availability of data. We examine the inertia measure α and link it with the efficiency of job markets.

¹<https://www.sec.gov/answers/execcomp.htm>

Sector	10	15	20	25	30	35	40	45	50	55	60
Spearman	0.72	0.793	0.752	0.515	0.755	0.768	0.745	0.646	0.75	0.871	0.559
Kendall	0.543	0.598	0.564	0.362	0.571	0.587	0.579	0.475	0.564	0.692	0.388

Table 1: Spearman and Kendall rank correlation between net sales and compensations in five years.

6 Executive job market

6.1 Overview

We focus on a five-year time horizon 2017 – 2021. The net sales data are from Compustat and the executive compensation information is from Execucomp. With the data cleaning procedure in Section B.1, our final sample consists of 790 firms, with a total market value of 61.7 trillion U.S. dollars in 2021. 396 firms are S&P 500 components. Table 7 in the e-companion presents the descriptive statistics for the data. Firms are classified into different industries using the Global Industry Classification Standard (GICS).

The first question we address is which industries are more aligned with the Roberts’ law, such that larger firms pay higher salaries to executives. To answer this question, we calculate the Spearman’s (Spearman, 1904) and Kendall’s (Kendall, 1938) rank correlations between net sales and compensations in Table 1. We find that the Consumer Discretionary (GICS Code 25), Real Estate (GICS Code 60), and Information Technology (GICS Code 45) industries are the top three sectors with weak correlations between net sales and wages. The Utilities industry (GICS Code 55) has the highest correlation.

Next, we examine the potential connection between the sale-wage correlation and inertia. In the following sections, we will calibrate the optimal value of α and find that the inertia is stronger when the relationship between sales and wages is weaker.

For clarity, we define an efficient job market as follows.

Definition 6.1. *A job market is said to be more efficient if the sale-wage correlation is higher. We call this correlation as the efficiency coefficient.*

Section 6.2 explains our choice of the statistical methods and Section 6.3 reports the main results.

6.2 Estimation methodology

6.2.1 Number of clusters

Ranks are discrete data that are suitable for discrete OT. However, the smallest number of firms in a single industry, as shown in Table 7, is 30. If we use the original ranks as the variables x_t and y_t , a large amount of data would be needed to estimate the transition probability matrices $\mu(dx_{t+1}|x_t)$ and $\nu(dy_{t+1}|y_t)$. This is unrealistic, as the earliest wage data in Execucomp is primarily from 1992. In addition, transitions of original ranks can be noisy and sensitive to fluctuations in the data. There is also a practical concern about the computational burden of a large transport plan matrix.

Therefore, we need to aggregate data into several clusters with orders. There are two questions to consider in this process: the number of clusters and whether to use even-sized or uneven-sized clusters. As for the first question, the number of clusters cannot be too small or too large. A small number of clusters fails to capture the variations in the data. If we use only one cluster, all industries would perfectly match firms with wages. On the other hand, using too many clusters leads to the problems discussed above. There is no theoretical result on the optimal number of

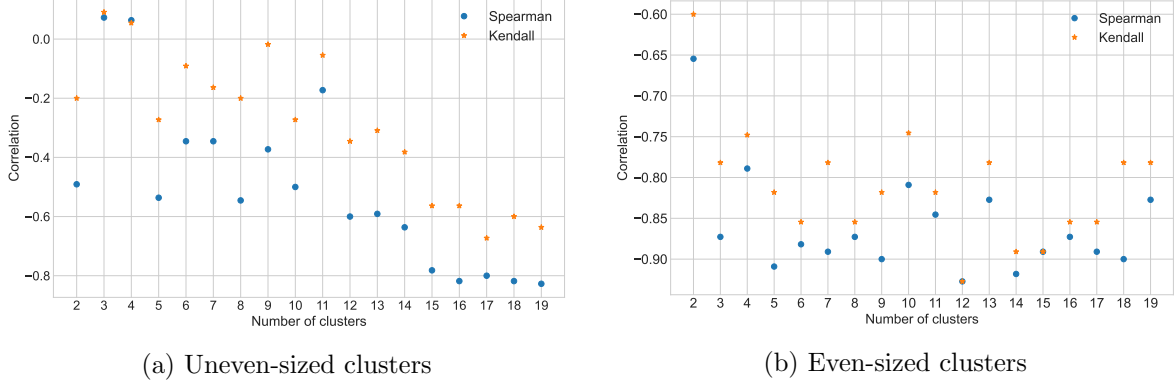


Figure 2: Selection for the optimal number of clusters.

clusters. Backhoff-Veraguas et al. (2022, Definition 1.2) suggests using $N^{1/(T+1)}$ clusters, where N is the number of time series. However, this result is only valid for $N \rightarrow \infty$, and would be too small when there are only a few data points. Given these difficulties, we suggest a practical and data-driven rule for determining the number of clusters.

For simplicity, we will use the same number of clusters for each industry to ensure fairness when comparing cross-sectional differences. The main feature we want to preserve after clustering is the relationship between sales and wages. Clusters are ordered and sales/wages in the same cluster are assigned with the same rank. Denote the sale and wage cluster ranks for the firm i at time t as x_t^i and y_t^i , respectively. We call the mean absolute value of the difference in wage and sale ranks, that is,

$$\frac{1}{NT} \sum_{i=1}^N \sum_{t=1}^T |x_t^i - y_t^i|,$$

as the *sale-wage discrepancy* for this industry. If the number of clusters is chosen properly, the sale-wage discrepancy should be bigger for sectors with lower sale-wage efficiency reported in Table 1. In other words, if we calculate the correlation between the sale-wage discrepancy and the sale-wage efficiency, we should prefer the number of clusters that generates strong negative correlations.

Figure 2 shows the correlations between the sale-wage discrepancy and efficiency using different numbers of clusters. The clusters are uneven in size in Figure 2a and even in size in Figure 2b. The uneven clusters are determined using the Jenks optimization method (Jenks, 1967) and the original values of wages and log values of sales. One advantage of uneven clusters is that the correlation is roughly monotonic with the number of clusters, as shown in Figure 2a. However, a disadvantage is that a large number of clusters is required to achieve a low, negative correlation, which is impractical due to the small amount of data. Even-sized clusters with ranks as the input, shown in Figure 2b, can achieve a low correlation with a relatively small number of clusters. Figure 2 reports both Kendall’s and Spearman’s rank correlations. We choose the first number of clusters that has a low enough correlation. Based on Figure 2b, the suitable number of clusters is 5 or 6, depending on the type of the correlation used. As a robustness check, we also report the results using seven clusters in the e-companion.

6.2.2 Estimation of transition matrices

After determining the number of clusters, we estimate the conditional probability kernels which are transition matrices of ranks. We impose the following assumption to further simplify the model

specification.

Assumption 6.2. *The conditional kernels $\mu(dx_{t+1}|x_{1:t})$ and $\nu(dy_{t+1}|y_{1:t})$ are Markov and time-homogeneous. That is, $\mu(dx_{t+1}|x_{1:t}) = \mu(dx_{t+1}|x_t)$ and is the same for any $t = 1, \dots, T - 1$. The same condition holds for $\nu(dy_{t+1}|y_{1:t})$ as well.*

To improve the accuracy of these estimates, we use wage-sale data spanning from 2010 to 2021 for the 790 firms considered in Table 7. We allow the planner to use all available data from 2010 to the final year of 2021 in the estimation process, in order to provide a larger pool of data. The transition matrices are calculated based on the frequencies of observed transitions between ranks over the years. Estimation results are given in Section B of the e-companion.

The transitions between ranks are crucial for our analysis. In the extreme case, $x_{t+1} = x_t$ and $y_{t+1} = y_t$ with probability one, that is, transition matrices are identity matrices. Then the state-dependent term will have no impact on the transport plans, because the marginal constraints have determined the matching already. There is no freedom to alter firm-wage pairs over time when rank transitions are forbidden. However, as long as transitions are not deterministic, we can capture α with enough data.

6.2.3 Model validation

To stabilize the calibration, we adopt two additional methods. First, as our real dataset is of limited size, we use the re-sampling technique (bootstrapping) to generate a larger dataset by drawing with replacement from the real samples. Second, in practice, there are only a few non-zero entries in the one-period transport plans π_t . However, after multiplying the one-period transport plans as in equation (1.3) to obtain $\pi(\alpha)$, there are many paths of $(x_{1:T}, y_{1:T})$ with very small probabilities. To speed up the calculation of the Wasserstein distance $\mathcal{W}(\pi(\alpha), \pi_r)$ in (5.6) and amplify the impact of α , we restrict the domain of $\pi(\alpha)$ to a set of paths with an equal size of the bootstrap samples and the highest probabilities.

In our model, several approximations and hyperparameters may cause systematic bias, including the number of clusters, estimation errors in the transition matrices, the choice of the state-dependent preference function, the size of the bootstrap samples, and the restriction of $\pi(\alpha)$ on paths with the highest probabilities. To address concerns about potential bias in our model, we propose to first apply it to synthetic data consisting only of perfectly matched sale-wage pairs. That is, firms ranked number n always pay wages ranked number n . In this case, $x_t = y_t$ for all time points $1 \leq t \leq T$. Ideally, we would expect to observe the optimal value of α to be close to zero in this scenario. There are several advantages to this validation procedure. First, it allows us to test whether the framework is functioning correctly in the simplest possible case. Second, it provides a method for selecting appropriate hyperparameters such that the benchmark outcome is close to zero. Finally, we can use the outcome of this analysis to correct any systematic bias in the model.

6.3 Results

Consider the number of clusters as 6 and the preference function as the indicator function. We divided the ranks by the number of clusters n , such that x_t and y_t are in $[0, 1 - 1/n]$, with 0 representing the highest rank. The candidate values for α are discrete and evenly spaced as $\{-1.5, -1.44, \dots, 0, \dots, 1.44, 1.5\}$, with a step size of 0.06. The discount factor is set to $\delta = 0.9$. We ran the calibration with ten simulation instances. The size of both the synthetic and bootstrap samples is set to 500. We restricted the domain of $\pi(\alpha)$ to 500 paths with the highest probabilities. The first row of Table 2, named as benchmark α , presents the mean values of the optimal α

Sector	10	15	20	25	30	35	40	45	50	55	60
Benchmark α	-0.084	-0.06	-0.06	-0.084	-0.042	-0.114	-0.288	-0.096	-0.258	-0.12	-0.06
Raw α	0.438	0.006	0.276	0.522	0.054	0.03	-0.048	0.66	-0.384	0.018	0.702
Adjusted α	0.522	0.066	0.336	0.606	0.096	0.144	0.24	0.756	-0.126	0.138	0.762

Table 2: Mean values of the optimal α in ten simulations. The number of clusters is set as 6. If there are multiple optimal α , we choose the one that is closest to zero.

with synthetic perfectly matched data. In most sectors, the optimal benchmark α is close to zero. Moreover, we observe that the model is biased toward the negative values of α . Next, we feed the model with bootstrap samples from the real dataset. The row labeled “raw α ” in Table 2 reports the optimal α obtained from the resampled real data. Most of these values shift to the positive direction. Sector 50 obtains a smaller value due to a small fluctuation in the Wasserstein distance. The last row in Table 2 calculates the difference between the raw and benchmark α . Overall, there is a state-dependent effect or inertia in most industries, regardless of whether the raw α or the adjusted α is used.

To understand the impact of α on the Wasserstein distance $\mathcal{W}(\pi(\alpha), \pi_r)$ between the model-implied and empirical transport plans, we consider the Materials and the Real Estate sectors as examples. Figures 3 and 4 depict the calibration curves with α as the horizontal axis and $\mathcal{W}(\pi(\alpha), \pi_r)$ in (5.6) (normalized) as the vertical axis. The Wasserstein distance is divided by $\mathcal{W}(\pi(-1.5), \pi_r)$ such that all curves start from 1 when $\alpha = -1.5$. There are ten curves in each subplot, representing ten simulation instances with independent bootstrap samples. When comparing the results in Figures 3a and 3b for the Materials sector (GICS Code 15), we find that the shape of the calibration curves does not change significantly when perfectly matched data are replaced by the resampled real data. This suggests that the Materials sector does not exhibit a significant state-dependent phenomenon or inertia in sale-wage pairs. However, in the Real Estate sector, we find that the inertia is strong. The optimal α shifts significantly toward positive values in Figure 4b, in contrast to the synthetic perfectly matched data in Figure 4a. Besides, the state-dependent term can reduce the Wasserstein distance on the negative side more effectively, indicating that negative values of α are less plausible.

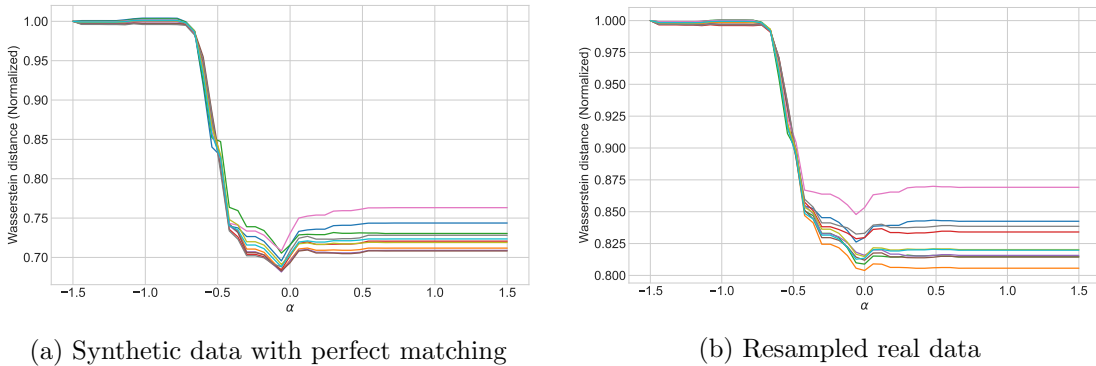


Figure 3: Calibration curves for Materials sector (GICS Code 15). Ten curves in each subplot represent ten independent simulations.

Correlation	Spearman (p -value)	Kendall (p -value)
Raw α	−0.645 (0.032)	−0.600 (0.010)
Adjusted α	−0.773 (0.005)	−0.600 (0.010)

Table 3: The relation between job market efficiency and the inertia effect. The correlations are between the optimal α in Table 2 and the sale-wage efficiency coefficient in Table 1. The number of clusters is 6.

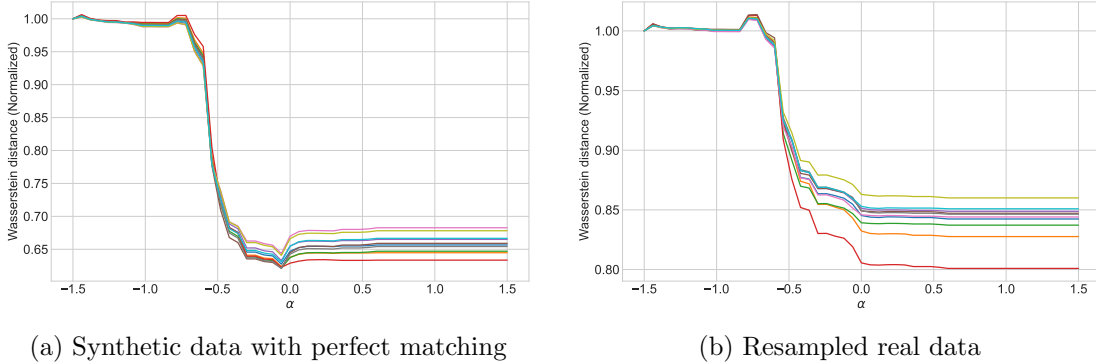


Figure 4: Calibration curves for Real Estate sector (GICS Code 60). Ten curves in each subplot represent ten independent simulations.

Main observation

The central message of this section is that sectors with less efficient job markets tend to exhibit a higher level of inertia. This assertion has been supported by the negative correlations between the optimal α in Table 2 and the sale-wage efficiency coefficient in Table 1. Table 3 shows that the correlation values are generally less than -0.6 and statistically significant at the 5% level. Job markets with stronger inertia are less likely to embrace the PAM and adapt to change. Thus, there is a negative relationship between job market efficiency and inertia within a dynamic framework. In Section B.3 of the e-companion, we conduct a robustness check with different numbers of clusters and obtain similar conclusions.

7 Academic job market

7.1 Overview

In contrast to the executive job market, the academic job market received less attention in the literature. Our analysis fills this gap using the University of California (UC) compensation data from the Government Compensation in California website [2] for the period of 2017 – 2021. The dataset includes total annual wages for various positions. In our analysis, we focus on four specific full-time positions: “Prof-Ay-B/E/E”, “Assoc Prof-Ay-B/E/E”, “Asst Prof-Ay-B/E/E”, and “Postdoc-Employee”. “AY” is short for Academic Year and “B/E/E” means Business/Economics/Engineering. In our current dataset, these three areas are reported jointly. The employees under the “Postdoc-Employee” title are from all departments. These full-time positions may provide a better representation of compensation levels than part-time positions. Tables 12 – 15 in the e-companion present

²<https://publicpay.ca.gov/Reports/RawExport.aspx>

Position	Professor	Associate Professor	Assistant Professor	Postdoc
Spearman	0.78	0.747	0.868	0.403
Kendall	0.616	0.585	0.707	0.298

Table 4: Correlations between university rankings and wages in 2017–2021.

the summary statistics of salaries in 2017 – 2021 for nine universities in the UC system, except UC San Francisco since it focuses on medical research and does not have faculty in the B/E/E departments. These tables also include the number of employees under each job title for 2021 only.

To quantify the quality of universities, we use the U.S. News rankings. There is a dataset with historical rankings collected by Andrew G. Reiter and available at his website [3]. It is worth noting that faculty salaries are included as a factor in these rankings, albeit with a weight of only 7% [4]. Therefore, faculty wages and university rankings are not the same automatically. To determine the annual pay levels at each university, we calculate a single value by first ranking all wage observations among a given year and job title, and then selecting the median rank as a measure of compensation levels. This method mitigates the impact of outliers in the data.

Table 4 presents Spearman’s and Kendall’s rank correlations between university rankings and wages in 2017 – 2021. Salaries for B/E/E assistant professors are more consistent with university rankings, compared with executives in most sectors. However, postdoc salaries do not show a strong positive correlation with university rankings. It is the lowest among all job positions and business sectors analyzed in this paper. This pattern motivates us to examine whether the inertia in postdoc salaries is also stronger.

7.2 Number of clusters and estimation of transition matrices

To determine the number of clusters for our analysis, we consider the U.S. News rankings and domain knowledge, as the small number of universities in our dataset (nine) makes it difficult to use the criterion applied to the executive data. We find that there are usually two universities with closely ranked positions, with the top two universities in the UC system ranking around the 20th place among national universities (and sometimes tied). The other universities tend to rank around the 30th, 40th, 80th, and 90th places. Based on these observations, we set the number of clusters to five, with two universities in each of the top four clusters and one university in the last cluster. Estimation results of the transition matrices are given in Figures 8 and 9 of the e-companion.

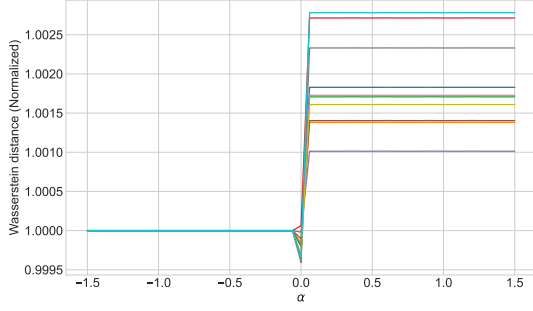
7.3 Results

Since the number of universities in our dataset is much smaller than the number of firms, we set the size of our bootstrap samples to 200 for each simulation. We use the state-dependent preference function with $\tau = 1$ and $\alpha \in \{-1.5, -1.44, \dots, 0, \dots, 1.44, 1.5\}$ evenly spaced with a step size of 0.06.

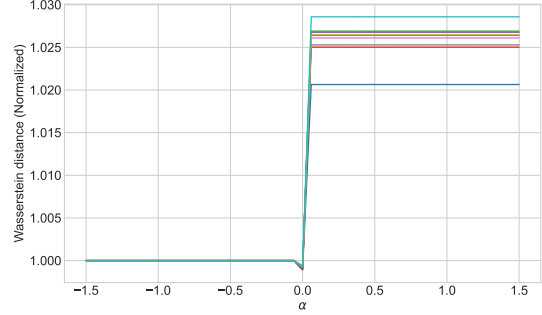
Using the B/E/E Professors data, Figure 5 plots the Wasserstein distance between the model-implied transport plan $\pi(\alpha)$ and the empirical transport plan π_r . The Wasserstein distance is divided by $\mathcal{W}(\pi(-1.5), \pi_r)$ such that all curves start from 1 when $\alpha = -1.5$. As a validation test and benchmark, Figure 5a calibrates α to synthetic data with perfect matching and plots curves from ten simulation instances. It shows that the optimal α is zero and there is no evidence of inertia when synthetic data with perfectly matching are used. In contrast, Figure 5b shows the results

³<https://andyreiter.com/datasets/>

⁴See the article at <https://www.usnews.com/education/best-colleges/articles/how-us-news-calculated-the-rankings>



(a) Synthetic data with perfect matching



(b) Resampled real data

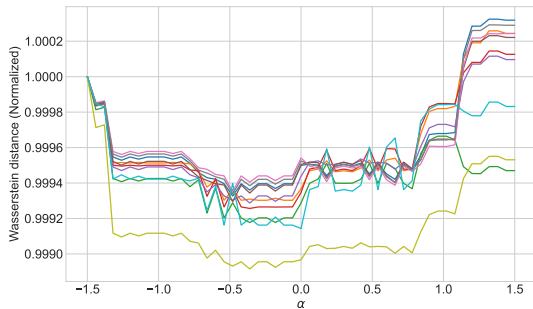
Figure 5: Calibration curves for B/E/E professors. In each subplot, ten curves represent individual calibrations with ten independent sampled data.

using bootstrap samples. The optimal α is still zero across different simulation runs, indicating that the real data for the professor category are very similar to the perfectly matched synthetic data. Table 5 reports the mean values of optimal α across these ten simulations.

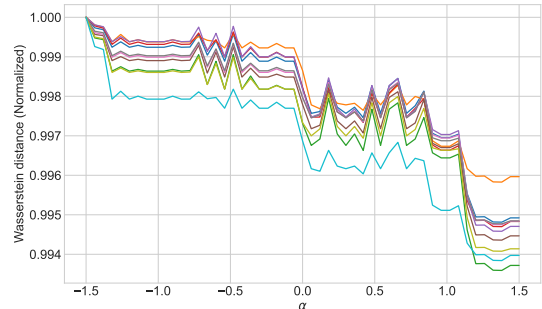
We observe similar curves for associate professors and assistant professors. Their wages are also highly matched with university rankings, with no significant evidence of inertia. We report the mean values of the optimal α in Table 5 and show the calibration curves in Figures 11 – 10, deferred to the e-companion.

Main observation

In contrast, we observe strong inertia in the salary data for postdocs. Figure 6a demonstrates the effectiveness of our framework by showing that the optimal α is close to zero when using synthetic perfectly matched data. However, when we use the bootstrap samples, the trend in the calibration curves changes significantly. Figure 6b shows that the optimal α exceeds 1, indicating strong inertia in the postdoc salary data. This effect is also stronger than in the executive data. The wages of postdocs do not match the rankings of universities. In the past five years from 2017 to 2021, UC Berkeley has paid lower median salaries to postdocs, compared with UCLA and several other universities in the UC system, as shown in Table 15. However, the difference in postdoc wages is small. Additionally, the change in Wasserstein distance is also small, mainly because the university wage data, with only nine observations, have a simpler structure than the executive data.



(a) Synthetic data with perfect matching



(b) Resampled real data

Figure 6: Calibration curves for postdocs.

Figure 6 also shows that the Wasserstein distance curves can be noisy when α varies. To estimate the optimal α robustly, we filter the original curves using the one-dimensional total variation denoising algorithm (Condat, 2013). This algorithm is suitable for signals with piecewise constant behaviors. Table 5 reports the mean optimal α calculated from the filtered data. There is no significant evidence of inertia in wages for tenured and tenure-track faculty. In contrast, the effect of inertia is very strong in the postdoc sector.

Position	Professor	Associate Professor	Assistant Professor	Postdoc
Benchmark α	0.0	−0.06	−0.06	0.0
Raw α	0.0	−0.06	−0.06	1.194
Adjusted α	0.0	0.0	0.0	1.194

Table 5: Mean values of optimal α after total variation filtering.

We test the connection between the inertia and university ranking-wage correlations, summarized in Table 6. Correlations in Table 6 are negative, showing that when the inertia is stronger, wages are less matched with university rankings. However, the power of our tests is low since only four types of jobs are considered.

Correlation	Spearman (p -value)	Kendall (p -value)
Raw α	−0.632 (0.368)	−0.548 (0.279)
Adjusted α	−0.775 (0.225)	−0.707 (0.180)

Table 6: Correlations between optimal α and the ranking-wage dependence.

References

- Acciaio, B., Backhoff-Veraguas, J., and Jia, J. (2021). Cournot–Nash equilibrium and optimal transport in a dynamic setting. *SIAM Journal on Control and Optimization*, 59(3):2273–2300.
- Acciaio, B., Backhoff-Veraguas, J., and Zalashko, A. (2020). Causal optimal transport and its links to enlargement of filtrations and continuous-time stochastic optimization. *Stochastic Processes and their Applications*, 130(5):2918–2953.
- Arjovsky, M., Chintala, S., and Bottou, L. (2017). Wasserstein generative adversarial networks. In *International Conference on Machine Learning*, pages 214–223. PMLR.
- Arora, R. and Gao, R. (2022). Data-driven multistage distributionally robust optimization with nested distance: Time consistency and tractable dynamic reformulations. *Optimization Online*. <https://optimization-online.org/?p=20641>.
- Backhoff-Veraguas, J., Bartl, D., Beiglböck, M., and Eder, M. (2020). Adapted Wasserstein distances and stability in mathematical finance. *Finance and Stochastics*, 24(3):601–632.
- Backhoff-Veraguas, J., Bartl, D., Beiglböck, M., and Wiesel, J. (2022). Estimating processes in adapted Wasserstein distance. *The Annals of Applied Probability*, 32(1):529–550.
- Backhoff-Veraguas, J., Beiglbock, M., Lin, Y., and Zalashko, A. (2017). Causal transport in discrete time and applications. *SIAM Journal on Optimization*, 27(4):2528–2562.

- Backhoff-Veraguas, J. and Zhang, X. (2023). Dynamic Cournot-Nash equilibrium: the non-potential case. *Mathematics and Financial Economics*, 17(2):153–174.
- Barberis, N. (2012). A model of casino gambling. *Management Science*, 58(1):35–51.
- Basak, S. and Chabakauri, G. (2010). Dynamic mean-variance asset allocation. *The Review of Financial Studies*, 23(8):2970–3016.
- Bayraktar, E., Eckstein, S., and Zhang, X. (2022). Stability and sample complexity of divergence regularized optimal transport. *arXiv preprint arXiv:2212.00367*.
- Bayraktar, E., Zhang, J., and Zhou, Z. (2021). Equilibrium concepts for time-inconsistent stopping problems in continuous time. *Mathematical Finance*, 31(1):508–530.
- Beiglböck, M., Jourdain, B., Margheriti, W., and Pammer, G. (2022). Approximation of martingale couplings on the line in the adapted weak topology. *Probability Theory and Related Fields*, 183(1):359–413.
- Bertsekas, D. and Shreve, S. E. (1978). *Stochastic optimal control: The discrete-time case*. Academic Press.
- Björk, T., Khapko, M., and Murgoci, A. (2017). On time-inconsistent stochastic control in continuous time. *Finance and Stochastics*, 21(2):331–360.
- Björk, T. and Murgoci, A. (2014). A theory of Markovian time-inconsistent stochastic control in discrete time. *Finance and Stochastics*, 18(3):545–592.
- Björk, T., Murgoci, A., and Zhou, X. Y. (2014). Mean-variance portfolio optimization with state-dependent risk aversion. *Mathematical Finance*, 24(1):1–24.
- Blanchet, J., Chen, L., and Zhou, X. Y. (2021a). Distributionally robust mean-variance portfolio selection with Wasserstein distances. *Management Science*.
- Blanchet, J. and Murthy, K. (2019). Quantifying distributional model risk via optimal transport. *Mathematics of Operations Research*, 44(2):565–600.
- Blanchet, J., Murthy, K., and Nguyen, V. A. (2021b). Statistical analysis of Wasserstein distributionally robust estimators. In *Tutorials in Operations Research: Emerging Optimization Methods and Modeling Techniques with Applications*, pages 227–254. INFORMS.
- Bogachev, V. I. (2007). *Measure Theory*, volume II. Springer Science & Business Media.
- Brenier, Y. (1991). Polar factorization and monotone rearrangement of vector-valued functions. *Communications on pure and applied mathematics*, 44(4):375–417.
- Brown, L. D. and Purves, R. (1973). Measurable selections of extrema. *The Annals of Statistics*, pages 902–912.
- Carlier, G. and Ekeland, I. (2010). Matching for teams. *Economic Theory*, 42:397–418.
- Charalambos, D. and Aliprantis, B. (2013). *Infinite Dimensional Analysis: A Hitchhiker’s Guide*. Springer.

- Chiappori, P.-A., McCann, R. J., and Nesheim, L. P. (2010). Hedonic price equilibria, stable matching, and optimal transport: equivalence, topology, and uniqueness. *Economic Theory*, 42:317–354.
- Condat, L. (2013). A direct algorithm for 1-D total variation denoising. *IEEE Signal Processing Letters*, 20(11):1054–1057.
- Cuturi, M. (2013). Sinkhorn distances: Lightspeed computation of optimal transport. *Advances in neural information processing systems*, 26.
- Delon, J. and Desolneux, A. (2020). A Wasserstein-type distance in the space of Gaussian mixture models. *SIAM Journal on Imaging Sciences*, 13(2):936–970.
- Demerjian, P., Lev, B., and McVay, S. (2012). Quantifying managerial ability: A new measure and validity tests. *Management Science*, 58(7):1229–1248.
- Epstein, L. G. and Ji, S. (2022). Optimal learning under robustness and time-consistency. *Operations Research*, 70(3):1317–1329.
- Föllmer, H. and Schied, A. (2011). *Stochastic finance: An introduction in discrete time*. Walter de Gruyter.
- Gabaix, X. and Landier, A. (2008). Why has CEO pay increased so much? *The Quarterly Journal of Economics*, 123(1):49–100.
- Galichon, A. (2016). *Optimal transport methods in economics*. Princeton University Press.
- Gangbo, W. and McCann, R. J. (1996). The geometry of optimal transportation. *Acta Mathematica*, 177(2):113–161.
- Gao, R. and Kleywegt, A. (2022). Distributionally robust stochastic optimization with Wasserstein distance. *Mathematics of Operations Research*.
- Han, B., Pun, C. S., and Wong, H. Y. (2021). Robust state-dependent mean–variance portfolio selection: A closed-loop approach. *Finance and Stochastics*, 25(3):529–561.
- Jenks, G. F. (1967). The data model concept in statistical mapping. *International Yearbook of Cartography*, 7:186–190.
- Kahneman, D. and Tversky, A. (1979). Prospect theory: An analysis of decision under risk. *Econometrica*, 47(2):263–292.
- Kallenberg, O. (2021). *Foundations of Modern Probability*. Springer Science & Business Media. The third edition.
- Kechris, A. (2012). *Classical descriptive set theory*, volume 156. Springer Science & Business Media.
- Kendall, M. G. (1938). A new measure of rank correlation. *Biometrika*, 30(1/2):81–93.
- Kováčová, G. and Rudloff, B. (2021). Time consistency of the mean-risk problem. *Operations research*, 69(4):1100–1117.
- Kuhn, D., Esfahani, P. M., Nguyen, V. A., and Shafieezadeh-Abadeh, S. (2019). Wasserstein distributionally robust optimization: Theory and applications in machine learning. In *Operations research & management science in the age of analytics*, pages 130–166. INFORMS.

- Laibson, D. (1997). Golden eggs and hyperbolic discounting. *The Quarterly Journal of Economics*, 112(2):443–478.
- Lassalle, R. (2013). Causal transference plans and their Monge-Kantorovich problems. *arXiv preprint arXiv:1303.6925*.
- Ma, J., Wong, T.-K. L., and Zhang, J. (2021). Time-consistent conditional expectation under probability distortion. *Mathematics of Operations Research*, 46(3):1149–1180.
- Mohajerin Esfahani, P. and Kuhn, D. (2018). Data-driven distributionally robust optimization using the Wasserstein metric: Performance guarantees and tractable reformulations. *Mathematical Programming*, 171(1):115–166.
- Neufeld, A. and Sester, J. (2021). On the stability of the martingale optimal transport problem: A set-valued map approach. *Statistics & Probability Letters*, 176:109131.
- Nguyen, V. A., Kuhn, D., and Mohajerin Esfahani, P. (2022). Distributionally robust inverse covariance estimation: The Wasserstein shrinkage estimator. *Operations Research*, 70(1):490–515.
- Parthasarathy, K. R. (2005). *Probability measures on metric spaces*, volume 352. American Mathematical Soc.
- Peyré, G. and Cuturi, M. (2019). Computational optimal transport: With applications to data science. *Foundations and Trends® in Machine Learning*, 11(5-6):355–607.
- Pflug, G. C. and Pichler, A. (2012). A distance for multistage stochastic optimization models. *SIAM Journal on Optimization*, 22(1):1–23.
- Pflug, G. C. and Pichler, A. (2014). *Multistage stochastic optimization*, volume 1104. Springer.
- Pichler, A., Liu, R. P., and Shapiro, A. (2022). Risk-averse stochastic programming: Time consistency and optimal stopping. *Operations Research*, 70(4):2439–2455.
- Schiebinger, G., Shu, J., Tabaka, M., Cleary, B., Subramanian, V., Solomon, A., Gould, J., Liu, S., Lin, S., Berube, P., et al. (2019). Optimal-transport analysis of single-cell gene expression identifies developmental trajectories in reprogramming. *Cell*, 176(4):928–943.
- Seguy, V., Damodaran, B. B., Flamary, R., Courty, N., Rolet, A., and Blondel, M. (2018). Large-scale optimal transport and mapping estimation. In *International Conference on Learning Representations*, pages 1–15.
- Spearman, C. (1904). The proof and measurement of association between two things. *The American Journal of Psychology*, 15(1):72–101.
- Strotz, R. (1955). Myopia and inconsistency in dynamic utility maximization. *Review of Economic Studies*, 23(3):165–180.
- Sundaram, R. K. (1996). *A first course in optimization theory*. Cambridge university press.
- Taşkesen, B., Shafieezadeh-Abadeh, S., and Kuhn, D. (2023). Semi-discrete optimal transport: Hardness, regularization and numerical solution. *Mathematical Programming*, 199(1-2):1033–1106.

- Taylor, L. A. (2013). CEO wage dynamics: Estimates from a learning model. *Journal of Financial Economics*, 108(1):79–98.
- Torous, W., Gunsilius, F., and Rigollet, P. (2021). An optimal transport approach to causal inference. *arXiv preprint arXiv:2108.05858*.
- Villani, C. (2009). *Optimal transport: old and new*, volume 338. Springer.
- Xu, T., Li, W. K., Munn, M., and Acciaio, B. (2020). COT-GAN: Generating sequential data via causal optimal transport. *Advances in Neural Information Processing Systems*, 33:8798–8809.

A Proofs of results

A.1 The semi-discrete and Markovian case

We need several auxiliary results to study the continuity. Lemmas A.1 and A.2 do not rely on any particular choice of the metric.

Lemma A.1. *Suppose*

- (1) $(\mathcal{X}_t, \mathcal{T}_{\mathcal{X}_t}), (\mathcal{X}_{t+1}, \mathcal{T}_{\mathcal{X}_{t+1}}), (\mathcal{Y}_t, \mathcal{T}_{\mathcal{Y}_t}), (\mathcal{Y}_{t+1}, \mathcal{T}_{\mathcal{Y}_{t+1}})$ are Polish topological spaces and the product spaces between them are endowed with product topologies;
- (2) the stochastic kernels $\mu(dx_{t+1}|x_t) : (\mathcal{X}_t, \mathcal{T}_{\mathcal{X}_t}) \rightarrow (\mathcal{P}(\mathcal{X}_{t+1}), \mathcal{V}[C_b(\mathcal{X}_{t+1}; \mathcal{T}_{\mathcal{X}_{t+1}})])$ and $\nu(dy_{t+1}|y_t) : (\mathcal{Y}_t, \mathcal{T}_{\mathcal{Y}_t}) \rightarrow (\mathcal{P}(\mathcal{Y}_{t+1}), \mathcal{V}[C_b(\mathcal{Y}_{t+1}; \mathcal{T}_{\mathcal{Y}_{t+1}})])$ are continuous.

Denote a correspondence as

$$D : (\mathcal{X}_t \times \mathcal{Y}_t, \mathcal{T}_{\mathcal{X}_t} \times \mathcal{T}_{\mathcal{Y}_t}) \rightarrow (\mathcal{P}(\mathcal{X}_{t+1} \times \mathcal{Y}_{t+1}), \mathcal{V}[C_b(\mathcal{X}_{t+1} \times \mathcal{Y}_{t+1}; \mathcal{T}_{\mathcal{X}_{t+1}} \times \mathcal{T}_{\mathcal{Y}_{t+1}})])$$

that maps $(x_t, y_t) \mapsto \Pi(\mu(dx_{t+1}|x_t), \nu(dy_{t+1}|y_t))$.

Then D is upper hemicontinuous and has non-empty, convex, and compact images. Moreover, D has a closed graph under the product topology $\mathcal{T}_{\mathcal{X}_t} \times \mathcal{T}_{\mathcal{Y}_t} \times \mathcal{V}[C_b(\mathcal{X}_{t+1} \times \mathcal{Y}_{t+1}; \mathcal{T}_{\mathcal{X}_{t+1}} \times \mathcal{T}_{\mathcal{Y}_{t+1}})]$.

Proof. $\Pi(\mu(dx_{t+1}|x_t), \nu(dy_{t+1}|y_t))$ is non-empty since the independent coupling belongs to this set. This set is convex. Indeed, if $\gamma^1, \gamma^2 \in \Pi(\mu(dx_{t+1}|x_t), \nu(dy_{t+1}|y_t))$, then $\lambda\gamma^1 + (1-\lambda)\gamma^2$, $\lambda \in [0, 1]$ is also a probability measure with marginals $\mu(dx_{t+1}|x_t)$ and $\nu(dy_{t+1}|y_t)$.

Since Polish spaces are second countable, first countable, and metrizable, we can apply Charalambos and Aliprantis (2013, Theorem 17.20). We only need to show that if a sequence $\{(x_t^n, y_t^n, \gamma^n)\}$ is in the graph of D and $(x_t^n, y_t^n) \rightarrow (x_t, y_t)$ under $\mathcal{T}_{\mathcal{X}_t} \times \mathcal{T}_{\mathcal{Y}_t}$, then the sequence $\{\gamma^n\}$ has a limit point in $\Pi(\mu(dx_{t+1}|x_t), \nu(dy_{t+1}|y_t))$.

We have assumed $\mu(dx_{t+1}|x_t)$ and $\nu(dy_{t+1}|y_t)$ are continuous with the usual weak convergence. Thus, by Prokhorov's theorem, $\{\mu(dx_{t+1}|x_t^n)\}_{n=1}^\infty$ and $\{\nu(dy_{t+1}|y_t^n)\}_{n=1}^\infty$ are tight. The set of couplings $\Pi(\{\mu(dx_{t+1}|x_t^n)\}_{n=1}^\infty, \{\nu(dy_{t+1}|y_t^n)\}_{n=1}^\infty)$ is also tight by Villani (2009, Lemma 4.4), where we emphasize that the product topology $\mathcal{T}_{\mathcal{X}_{t+1}} \times \mathcal{T}_{\mathcal{Y}_{t+1}}$ is imposed. Indeed, Villani (2009, Lemma 4.4) relies on the fact that, if $A \subset \mathcal{X}_{t+1}$ and $B \subset \mathcal{Y}_{t+1}$ are compact, then $A \times B$ is compact under the product topology $\mathcal{T}_{\mathcal{X}_{t+1}} \times \mathcal{T}_{\mathcal{Y}_{t+1}}$.

Since $\{\gamma^n\}_{n=1}^\infty$ is in $\Pi(\{\mu(dx_{t+1}|x_t^n)\}_{n=1}^\infty, \{\nu(dy_{t+1}|y_t^n)\}_{n=1}^\infty)$, we can apply Prokhorov's theorem again. A subsequence $\{\gamma^{n_k}\}_{k=1}^\infty$ converges weakly in the usual sense to some γ . We show $\gamma \in \Pi(\mu(dx_{t+1}|x_t), \nu(dy_{t+1}|y_t))$. Denote the projection operator on the first and second component

as $p_{\mathcal{X}} : \mathcal{X}_{t+1} \times \mathcal{Y}_{t+1} \rightarrow \mathcal{X}_{t+1}$ and $p_{\mathcal{Y}} : \mathcal{X}_{t+1} \times \mathcal{Y}_{t+1} \rightarrow \mathcal{Y}_{t+1}$. With the product topology, these projection operators are continuous. Hence, if $f(x_{t+1})$ is a $\mathcal{T}_{\mathcal{X}_{t+1}}$ -continuous function, then $f \circ p_{\mathcal{X}}$ is $\mathcal{T}_{\mathcal{X}_{t+1}} \times \mathcal{T}_{\mathcal{Y}_{t+1}}$ -continuous. Therefore, we have

$$\gamma^{n_k} \circ p_{\mathcal{X}}^{-1} \rightarrow \gamma \circ p_{\mathcal{X}}^{-1}, \quad \gamma^{n_k} \circ p_{\mathcal{Y}}^{-1} \rightarrow \gamma \circ p_{\mathcal{Y}}^{-1} \text{ weakly for } k \rightarrow \infty.$$

Since the marginals satisfy $\gamma^{n_k} \circ p_{\mathcal{X}}^{-1} = \mu(dx_{t+1}|x_t^{n_k})$ and $\gamma^{n_k} \circ p_{\mathcal{Y}}^{-1} = \nu(dy_{t+1}|y_t^{n_k})$, then together with $\mu(dx_{t+1}|x_t^{n_k}) \rightarrow \mu(dx_{t+1}|x_t)$, $\nu(dy_{t+1}|y_t^{n_k}) \rightarrow \nu(dy_{t+1}|y_t)$ weakly for $k \rightarrow \infty$, we obtain $\gamma \circ p_{\mathcal{X}}^{-1} = \mu(dx_{t+1}|x_t)$ and $\gamma \circ p_{\mathcal{Y}}^{-1} = \nu(dy_{t+1}|y_t)$. Therefore, $\gamma \in \Pi(\mu(dx_{t+1}|x_t), \nu(dy_{t+1}|y_t))$.

By Charalambos and Aliprantis (2013, Theorem 17.20), D is upper hemicontinuous and compact-valued. By Charalambos and Aliprantis (2013, Theorem 17.10) and Polish spaces are Hausdorff, D has a closed graph. \square

Lemma A.2. Consider Polish topological spaces $(\mathcal{S}_1, \mathcal{T}_{\mathcal{S}_1})$, $(\mathcal{S}_2, \mathcal{T}_{\mathcal{S}_2})$, and $(\mathcal{S}_3, \mathcal{T}_{\mathcal{S}_3})$. Suppose

- (1) the stochastic kernel $\gamma(ds_2|s_1) : (\mathcal{S}_1, \mathcal{T}_{\mathcal{S}_1}) \rightarrow (\mathcal{P}(\mathcal{S}_2), \mathcal{V}[C_b(\mathcal{S}_2; \mathcal{T}_{\mathcal{S}_2})])$ is continuous;
- (2) the function $h(s_3, s_2) : (\mathcal{S}_3 \times \mathcal{S}_2, \mathcal{T}_{\mathcal{S}_3} \times \mathcal{T}_{\mathcal{S}_2}) \rightarrow (\mathbb{R}, \mathcal{T}_{\mathbb{R}})$ is continuous and bounded.

Then

- (a) $\int_{\mathcal{S}_2} h(s_3, s_2) \gamma(ds_2|s_1)$ is $\mathcal{T}_{\mathcal{S}_3} \times \mathcal{T}_{\mathcal{S}_1}$ -continuous. If $(\mathcal{S}_3, \mathcal{T}_{\mathcal{S}_3}) = (\mathcal{S}_1, \mathcal{T}_{\mathcal{S}_1})$, it is understood as $\mathcal{T}_{\mathcal{S}_1}$ -continuous;
- (b) with $\lambda \in \mathcal{P}(\mathcal{S}_2)$, $\int_{\mathcal{S}_2} h(s_3, s_2) \lambda(ds_2)$ is $\mathcal{T}_{\mathcal{S}_3} \times \mathcal{V}[C_b(\mathcal{S}_2; \mathcal{T}_{\mathcal{S}_2})]$ -continuous.

Proof. Consider a sequence (s_3^n, s_1^n) converging to (s_3, s_1) under the product topology $\mathcal{T}_{\mathcal{S}_3} \times \mathcal{T}_{\mathcal{S}_1}$. Equip \mathcal{S}_1 , \mathcal{S}_2 , and \mathcal{S}_3 with some complete compatible metrics. $B := \{(s_3^n, s_1^n)\}_{n=1}^{\infty} \cup \{(s_3, s_1)\}$ is a compact set. Moreover, the uniform continuity is defined under these metrics.

Fix an arbitrary $\varepsilon > 0$. Since the product topology is used, then $s_1^n \rightarrow s_1$ under $\mathcal{T}_{\mathcal{S}_1}$. With the assumption that $\gamma(ds_2|s_1)$ is continuous in s_1 , $\gamma(ds_2|s_1^n)$ converges weakly to $\gamma(ds_2|s_1)$. Thus $\{\gamma(ds_2|s_1^n)\}_{n=1}^{\infty}$ is tight by Prokhorov's theorem. We can find a compact subset $A \subset \mathcal{S}_2$ such that $\sup_n \gamma(\mathcal{S}_2 \setminus A | s_1^n) \leq \varepsilon$.

Since h is uniformly continuous on the compact set $B \times A$, then there exists $N > 0$ such that

$$\sup_{n > N, s_2 \in A} |h(s_3, s_2) - h(s_3^n, s_2)| \leq \varepsilon. \quad (\text{A.1})$$

We have

$$\left| \int_{\mathcal{S}_2} h(s_3^n, s_2) \gamma(ds_2|s_1^n) - \int_{\mathcal{S}_2} h(s_3, s_2) \gamma(ds_2|s_1) \right| \leq \text{I} + \text{II} + \text{III},$$

where

$$\begin{aligned} \text{I} &= \left| \int_{\mathcal{S}_2} h(s_3, s_2) [\gamma(ds_2|s_1^n) - \gamma(ds_2|s_1)] \right|, \\ \text{II} &= \left| \int_A [h(s_3^n, s_2) - h(s_3, s_2)] \gamma(ds_2|s_1^n) \right|, \\ \text{III} &= \left| \int_{\mathcal{S}_2 \setminus A} [h(s_3^n, s_2) - h(s_3, s_2)] \gamma(ds_2|s_1^n) \right|. \end{aligned}$$

Since h is bounded and continuous, then the term I converges to zero thanks to the weak convergence. As the set A is compact, when $n > N$, we have $\text{II} \leq \varepsilon$ by the uniform continuity. $\text{III} \leq C\varepsilon$ for a generic constant C , since h is bounded and $\sup_n \gamma(\mathcal{S}_2 \setminus A | s_1^n) \leq \varepsilon$. As $\varepsilon > 0$ is arbitrary, we obtain the continuity as desired.

Claim (b) can be proved similarly. \square

Proof of Theorem 3.3

Proof. Recalling the $\pi^{t,\gamma}$ in Definition 2.1 but with a generic bicausal π after $t+1$, we can show a recursive relationship for the objective J in (3.1):

$$\begin{aligned} J(x_t, y_t; \pi^{t,\gamma}) = & \left[\int \left(c_{t+1}(x_t, y_t, x_{t+1}, y_{t+1}) + J(x_{t+1}, y_{t+1}; \pi) \right) \gamma(dx_{t+1}, dy_{t+1}) \right. \\ & - \int G\left(x_{t+1}, y_{t+1}, \int h(x_T, y_T) \pi(dx_T, dy_T | x_{t+1}, y_{t+1})\right) \gamma(dx_{t+1}, dy_{t+1}) \\ & + G\left(x_t, y_t, \int \int h(x_T, y_T) \pi(dx_T, dy_T | x_{t+1}, y_{t+1}) \gamma(dx_{t+1}, dy_{t+1})\right) \\ & - \int \int \sum_{k=t+2}^T c_k(x_{t+1}, y_{t+1}, x_k, y_k) \pi(dx_{t+2:T}, dy_{t+2:T} | x_{t+1}, y_{t+1}) \gamma(dx_{t+1}, dy_{t+1}) \\ & \left. + \int \int \sum_{k=t+2}^T c_k(x_t, y_t, x_k, y_k) \pi(dx_{t+2:T}, dy_{t+2:T} | x_{t+1}, y_{t+1}) \gamma(dx_{t+1}, dy_{t+1}) \right]. \end{aligned}$$

The proof is similar to the discrete case. Hence, if an equilibrium transport π^* exists and set $\pi = \pi^*$ for $t+1, \dots, T-1$, we can derive the extended DP equation (3.2) with the definitions of g_{t+1} and b_k . Next, we proceed by backward induction to show that the extended DP equation (3.2) is well-defined and V_t , g_{t+1} , and b_k are continuous under a finer Polish topology.

Consider time $t = T-1$. Since $\nu(dy_T | y_{T-1})$ is Borel measurable, Kechris (2012, Theorem 13.11) shows that there exists a finer Polish topology $\mathcal{T}_{\mathcal{Y}_{T-1}}^{(1)} \supseteq \mathcal{T}_{\mathcal{Y}_{T-1}}$ with the same Borel sets $\mathcal{B}(\mathcal{T}_{\mathcal{Y}_{T-1}}^{(1)}) = \mathcal{B}(\mathcal{T}_{\mathcal{Y}_{T-1}})$, such that $\nu(dy_T | y_{T-1}) : (\mathcal{Y}_{T-1}, \mathcal{T}_{\mathcal{Y}_{T-1}}^{(1)}) \rightarrow (\mathcal{P}(\mathcal{Y}_T), \mathcal{V}[C_b(\mathcal{Y}_T; \mathcal{T}_{\mathcal{Y}_T})])$ is continuous. Since previous open sets are still open, $\mathcal{T}_{\mathcal{Y}_{T-1}}$ -continuous functions are still $\mathcal{T}_{\mathcal{Y}_{T-1}}^{(1)}$ -continuous. We check that Brown and Purves (1973, Corollary 1) is applicable to our problem. By Lemma A.2 and Assumption 3.1, the objective at time $T-1$, given by

$$f(x_{T-1}, y_{T-1}, \gamma) := \int c_T(x_{T-1}, y_{T-1}, x_T, y_T) \gamma(dx_T, dy_T) + G\left(x_{T-1}, y_{T-1}, \int h(x_T, y_T) \gamma(dx_T, dy_T)\right),$$

is $\mathcal{T}_{\mathcal{X}_{T-1}} \times \mathcal{T}_{\mathcal{Y}_{T-1}}^{(1)} \times \mathcal{V}[C_b(\mathcal{X}_T \times \mathcal{Y}_T; \mathcal{T}_{\mathcal{X}_T} \times \mathcal{T}_{\mathcal{Y}_T})]$ -continuous.

By Lemma A.1, the graph of the correspondence

$$\begin{aligned} D : (\mathcal{X}_{T-1} \times \mathcal{Y}_{T-1}, \mathcal{T}_{\mathcal{X}_{T-1}} \times \mathcal{T}_{\mathcal{Y}_{T-1}}^{(1)}) & \rightarrow (\mathcal{P}(\mathcal{X}_T \times \mathcal{Y}_T), \mathcal{V}[C_b(\mathcal{X}_T \times \mathcal{Y}_T; \mathcal{T}_{\mathcal{X}_T} \times \mathcal{T}_{\mathcal{Y}_T})]) \\ & \text{that maps } (x_{T-1}, y_{T-1}) \mapsto \Pi(\mu(dx_T | x_{T-1}), \nu(dy_T | y_{T-1})), \end{aligned}$$

is closed and thus Borel. Therefore, the objective at time $T-1$ is defined on a Borel set. Moreover, for each (x_{T-1}, y_{T-1}) , the section $\Pi(\mu(dx_T | x_{T-1}), \nu(dy_T | y_{T-1}))$ is compact.

Therefore, by Brown and Purves (1973, Corollary 1), there is a Borel measurable optimizer $\pi^*(dx_T, dy_T | x_{T-1}, y_{T-1})$ such that

$$f(x_{T-1}, y_{T-1}, \pi^*(dx_T, dy_T | x_{T-1}, y_{T-1})) = \inf_{\gamma \in \Pi(\mu(dx_T | x_{T-1}), \nu(dy_T | y_{T-1}))} f(x_{T-1}, y_{T-1}, \gamma),$$

which is also the value function $V_{T-1}(x_{T-1}, y_{T-1})$.

As a preparation for applying Brown and Purves (1973, Corollary 1) at time $T-2$, we refine the topology on \mathcal{Y}_{T-1} again. Since \mathcal{X}_{T-1} is finite, we suppose $\mathcal{X}_{T-1} = \{1, \dots, n\}$ without loss of generality. For a given $i \in \mathcal{X}_{T-1}$, we apply Kechris (2012, Theorem 13.11) recursively to

$$\pi^*(dx_T, dy_T | i, y_{T-1}) : (\mathcal{Y}_{T-1}, \mathcal{T}_{\mathcal{Y}_{T-1}}^{(i)}) \rightarrow (\mathcal{P}(\mathcal{X}_T \times \mathcal{Y}_T), \mathcal{V}[C_b(\mathcal{X}_T \times \mathcal{Y}_T; \mathcal{T}_{\mathcal{X}_T} \times \mathcal{T}_{\mathcal{Y}_T})]).$$

There exists a stronger Polish topology $\mathcal{T}_{\mathcal{Y}_{T-1}}^{(i+1)} \supseteq \mathcal{T}_{\mathcal{Y}_{T-1}}^{(i)}$ with $\mathcal{B}(\mathcal{T}_{\mathcal{Y}_{T-1}}^{(i+1)}) = \mathcal{B}(\mathcal{T}_{\mathcal{Y}_{T-1}}^{(i)}) = \mathcal{B}(\mathcal{T}_{\mathcal{Y}_{T-1}})$, such that $\pi^*(dx_T, dy_T|i, y_{T-1})$ is $\mathcal{T}_{\mathcal{Y}_{T-1}}^{(i+1)}$ -continuous in y_{T-1} . We claim that $\pi^*(dx_T, dy_T|x_{T-1}, y_{T-1})$ is jointly continuous in (x_{T-1}, y_{T-1}) under the product topology $\mathcal{T}_{\mathcal{X}_{T-1}} \times \mathcal{T}_{\mathcal{Y}_{T-1}}^{(n+1)}$. Consider a complete compatible metric $d_{\mathcal{Y}}$ for $\mathcal{T}_{\mathcal{Y}_{T-1}}^{(n+1)}$ and the discrete metric $d_{\mathcal{X}}$ on \mathcal{X}_{T-1} , that is, $d_{\mathcal{X}}(x, x') = 0$ if $x = x'$ and $d_{\mathcal{X}}(x, x') = 1$ if $x \neq x'$. $(\mathcal{X}_{T-1} \times \mathcal{Y}_{T-1}, \mathcal{T}_{\mathcal{X}_{T-1}} \times \mathcal{T}_{\mathcal{Y}_{T-1}}^{(n+1)})$ is a Polish space with the metric $d_{\mathcal{X}}(x, x') + d_{\mathcal{Y}}(y, y')$, where we omitted the time subscript for simplicity. Denote $d_{\mathcal{P}}$ as a complete compatible metric for $(\mathcal{P}(\mathcal{X}_T \times \mathcal{Y}_T), \mathcal{V}[C_b(\mathcal{X}_T \times \mathcal{Y}_T; \mathcal{T}_{\mathcal{X}_T} \times \mathcal{T}_{\mathcal{Y}_T})])$. Given (x, y) , for every $\varepsilon > 0$, we want to show that there exists $\delta > 0$, such that if $d_{\mathcal{X}}(x, x') + d_{\mathcal{Y}}(y, y') < \delta$, then $d_{\mathcal{P}}(\pi^*(\cdot|x, y), \pi^*(\cdot|x', y')) < \varepsilon$. In fact, since for each $i \in \mathcal{X}_{T-1}$, we can find $\delta_i > 0$, such that if $d_{\mathcal{Y}}(y, y') < \delta_i$, then $d_{\mathcal{P}}(\pi^*(\cdot|i, y), \pi^*(\cdot|i, y')) < \varepsilon$. Therefore, we can take $\delta = \min\{\min_i\{\delta_i\}, 1\}$, which guarantees $x = x'$ when $d_{\mathcal{X}}(x, x') + d_{\mathcal{Y}}(y, y') < \delta$ and then apply the continuity on y under a fixed x to show $d_{\mathcal{P}}(\pi^*(\cdot|x, y), \pi^*(\cdot|x', y')) < \varepsilon$.

Moreover, by Lemma A.2,

$$g_{T-1}(x_{T-1}, y_{T-1}) := \int h(x_T, y_T) \pi^*(dx_T, dy_T|x_{T-1}, y_{T-1}),$$

$$b_T(x_{T-1}, y_{T-1}, x_{T-1}, y_{T-1}) := \int c_T(x_{T-1}, y_{T-1}, x_T, y_T) \pi^*(dx_T, dy_T|x_{T-1}, y_{T-1}),$$

and the value function $V_{T-1}(x_{T-1}, y_{T-1})$ are $\mathcal{T}_{\mathcal{X}_{T-1}} \times \mathcal{T}_{\mathcal{Y}_{T-1}}^{(n+1)}$ -continuous. For $i \in \{0, \dots, T-2\}$,

$$b_T(x_i, y_i, x_{T-1}, y_{T-1}) := \int c_T(x_i, y_i, x_T, y_T) \pi^*(dx_T, dy_T|x_{T-1}, y_{T-1})$$

is $\mathcal{T}_{\mathcal{X}_i} \times \mathcal{T}_{\mathcal{Y}_i} \times \mathcal{T}_{\mathcal{X}_{T-1}} \times \mathcal{T}_{\mathcal{Y}_{T-1}}^{(n+1)}$ -continuous.

At time $t = T-2$, \mathcal{Y}_{T-1} is always endowed with $\mathcal{T}_{\mathcal{Y}_{T-1}}^{(n+1)}$. By Bertsekas and Shreve (1978, Proposition 7.25) or Kechris (2012, Theorem 17.24), topological spaces $(\mathcal{P}(\mathcal{Y}_{T-1}), \mathcal{V}[C_b(\mathcal{Y}_{T-1}; \mathcal{T}_{\mathcal{Y}_{T-1}})])$ and $(\mathcal{P}(\mathcal{Y}_{T-1}), \mathcal{V}[C_b(\mathcal{Y}_{T-1}; \mathcal{T}_{\mathcal{Y}_{T-1}}^{(n+1)})])$ have the same collection of Borel sets, since $\mathcal{B}(\mathcal{T}_{\mathcal{Y}_{T-1}}^{(n+1)}) = \mathcal{B}(\mathcal{T}_{\mathcal{Y}_{T-1}})$. Hence, $\nu(dy_{T-1}|y_{T-2}) : (\mathcal{Y}_{T-2}, \mathcal{T}_{\mathcal{Y}_{T-2}}) \rightarrow (\mathcal{P}(\mathcal{Y}_{T-1}), \mathcal{V}[C_b(\mathcal{Y}_{T-1}; \mathcal{T}_{\mathcal{Y}_{T-1}}^{(n+1)})])$ is still Borel measurable. Similarly, by Kechris (2012, Theorem 13.11), there exists a finer Polish topology $\mathcal{T}_{\mathcal{Y}_{T-2}}^{(1)} \supseteq \mathcal{T}_{\mathcal{Y}_{T-2}}$ with the same Borel sets $\mathcal{B}(\mathcal{T}_{\mathcal{Y}_{T-2}}^{(1)}) = \mathcal{B}(\mathcal{T}_{\mathcal{Y}_{T-2}})$, such that $\nu(dy_{T-1}|y_{T-2}) : (\mathcal{Y}_{T-2}, \mathcal{T}_{\mathcal{Y}_{T-2}}^{(1)}) \rightarrow (\mathcal{P}(\mathcal{Y}_{T-1}), \mathcal{V}[C_b(\mathcal{Y}_{T-1}; \mathcal{T}_{\mathcal{Y}_{T-1}}^{(n+1)})])$ is continuous.

By Lemma A.2 and continuity results of V_{T-1} , g_{T-1} , and b_T above, the objective at time $T-2$, given by

$$\begin{aligned} f(x_{T-2}, y_{T-2}, \gamma) &:= \int \left(c_{T-1}(x_{T-2}, y_{T-2}, x_{T-1}, y_{T-1}) + V_{T-1}(x_{T-1}, y_{T-1}) \right) \gamma(dx_{T-1}, dy_{T-1}) \\ &\quad - \int G(x_{T-1}, y_{T-1}, g_{T-1}(x_{T-1}, y_{T-1})) \gamma(dx_{T-1}, dy_{T-1}) \\ &\quad + G\left(x_{T-2}, y_{T-2}, \int g_{T-1}(x_{T-1}, y_{T-1}) \gamma(dx_{T-1}, dy_{T-1})\right) \\ &\quad - \int b_T(x_{T-1}, y_{T-1}, x_{T-1}, y_{T-1}) \gamma(dx_{T-1}, dy_{T-1}) \\ &\quad + \int b_T(x_{T-2}, y_{T-2}, x_{T-1}, y_{T-1}) \gamma(dx_{T-1}, dy_{T-1}), \end{aligned}$$

is $\mathcal{T}_{\mathcal{X}_{T-2}} \times \mathcal{T}_{\mathcal{Y}_{T-2}}^{(1)} \times \mathcal{V}[C_b(\mathcal{X}_{T-1} \times \mathcal{Y}_{T-1}; \mathcal{T}_{\mathcal{X}_{T-1}} \times \mathcal{T}_{\mathcal{Y}_{T-1}}^{(n+1)})]$ -continuous.

By Lemma A.1, the correspondence

$$D : (\mathcal{X}_{T-2} \times \mathcal{Y}_{T-2}, \mathcal{T}_{\mathcal{X}_{T-2}} \times \mathcal{T}_{\mathcal{Y}_{T-2}}^{(1)}) \rightharpoonup (\mathcal{P}(\mathcal{X}_{T-1} \times \mathcal{Y}_{T-1}), \mathcal{V}[C_b(\mathcal{X}_{T-1} \times \mathcal{Y}_{T-1}; \mathcal{T}_{\mathcal{X}_{T-1}} \times \mathcal{T}_{\mathcal{Y}_{T-1}}^{(n+1)})])$$

that maps $(x_{T-2}, y_{T-2}) \mapsto \Pi(\mu(dx_{T-1}|x_{T-2}), \nu(dy_{T-1}|y_{T-2}))$,

has a closed graph and is compact-valued.

Again, Brown and Purves (1973, Corollary 1) proves that there exists a Borel measurable optimizer $\pi^*(dx_{T-1}, dy_{T-1}|x_{T-2}, y_{T-2})$ such that

$$f(x_{T-2}, y_{T-2}, \pi^*(dx_{T-1}, dy_{T-1}|x_{T-2}, y_{T-2})) = \inf_{\gamma \in \Pi(\mu(dx_{T-1}|x_{T-2}), \nu(dy_{T-1}|y_{T-2}))} f(x_{T-2}, y_{T-2}, \gamma),$$

which also gives the value function $V_{T-2}(x_{T-2}, y_{T-2})$.

Without loss of generality, suppose $\mathcal{X}_{T-2} = \{1, \dots, n\}$. There exists a finer topology $\mathcal{T}_{\mathcal{Y}_{T-2}}^{(n+1)} \supseteq \mathcal{T}_{\mathcal{Y}_{T-2}}$ with $\mathcal{B}(\mathcal{T}_{\mathcal{Y}_{T-2}}^{(n+1)}) = \mathcal{B}(\mathcal{T}_{\mathcal{Y}_{T-2}})$, such that $\pi^*(dx_{T-1}, dy_{T-1}|x_{T-2}, y_{T-2})$ is jointly continuous in (x_{T-2}, y_{T-2}) under the product topology $\mathcal{T}_{\mathcal{X}_{T-2}} \times \mathcal{T}_{\mathcal{Y}_{T-2}}^{(n+1)}$. Moreover,

$$\begin{aligned} g_{T-2}(x_{T-2}, y_{T-2}) &:= \int g_{T-1}(x_{T-1}, y_{T-1}) \pi^*(dx_{T-1}, dy_{T-1}|x_{T-2}, y_{T-2}), \\ b_{T-1}(x_{T-2}, y_{T-2}, x_{T-2}, y_{T-2}) &:= \int c_{T-1}(x_{T-2}, y_{T-2}, x_{T-1}, y_{T-1}) \pi^*(dx_{T-1}, dy_{T-1}|x_{T-2}, y_{T-2}), \\ &\int b_T(x_{T-1}, y_{T-1}, x_{T-1}, y_{T-1}) \pi^*(dx_{T-1}, dy_{T-1}|x_{T-2}, y_{T-2}), \\ &\int b_T(x_{T-2}, y_{T-2}, x_{T-1}, y_{T-1}) \pi^*(dx_{T-1}, dy_{T-1}|x_{T-2}, y_{T-2}), \end{aligned}$$

and the value function $V_{T-2}(x_{T-2}, y_{T-2})$ are $\mathcal{T}_{\mathcal{X}_{T-2}} \times \mathcal{T}_{\mathcal{Y}_{T-2}}^{(n+1)}$ -continuous. For $i \in \{0, \dots, T-3\}$,

$$\begin{aligned} b_{T-1}(x_i, y_i, x_{T-2}, y_{T-2}) &:= \int c_{T-1}(x_i, y_i, x_{T-1}, y_{T-1}) \pi^*(dx_{T-1}, dy_{T-1}|x_{T-2}, y_{T-2}) \\ \text{and } \int b_T(x_i, y_i, x_{T-1}, y_{T-1}) \pi^*(dx_{T-1}, dy_{T-1}|x_{T-2}, y_{T-2}) \end{aligned}$$

are $\mathcal{T}_{\mathcal{X}_i} \times \mathcal{T}_{\mathcal{Y}_i} \times \mathcal{T}_{\mathcal{X}_{T-2}} \times \mathcal{T}_{\mathcal{Y}_{T-2}}^{(n+1)}$ -continuous.

Therefore, we can prove the result by backward induction. $\pi^*(dx_{t+1}, dy_{t+1}|x_t, y_t)$ and $V_t(x_t, y_t)$ are Borel measurable. Indeed, there is a finer Polish topology such that they are continuous. \square

The proof of Corollary 3.5 needs the following properties of l.s.c. functions.

Corollary A.3. Consider Polish topological spaces $(\mathcal{S}_1, \mathcal{T}_{\mathcal{S}_1})$, $(\mathcal{S}_2, \mathcal{T}_{\mathcal{S}_2})$, and $(\mathcal{S}_3, \mathcal{T}_{\mathcal{S}_3})$. Suppose

- (1) the stochastic kernel $\gamma(ds_2|s_1) : (\mathcal{S}_1, \mathcal{T}_{\mathcal{S}_1}) \rightarrow (\mathcal{P}(\mathcal{S}_2), \mathcal{V}[C_b(\mathcal{S}_2; \mathcal{T}_{\mathcal{S}_2})])$ is continuous;
- (2) the function $h(s_3, s_2) : (\mathcal{S}_3 \times \mathcal{S}_2, \mathcal{T}_{\mathcal{S}_3} \times \mathcal{T}_{\mathcal{S}_2}) \rightarrow (\mathbb{R}, \mathcal{T}_{\mathbb{R}})$ is l.s.c. and bounded from below;
- (3) the function $g(s_2) : (\mathcal{S}_2, \mathcal{T}_{\mathcal{S}_2}) \rightarrow (\mathbb{R}, \mathcal{T}_{\mathbb{R}})$ is l.s.c. The function $G(s_1, g) : (\mathcal{S}_1 \times \mathbb{R}, \mathcal{T}_{\mathcal{S}_1} \times \mathcal{T}_{\mathbb{R}}) \rightarrow (\mathbb{R}, \mathcal{T}_{\mathbb{R}})$ is l.s.c. Moreover, $G(s_1, \cdot)$ is nondecreasing for each s_1 .

Then

- (a) $\int_{\mathcal{S}_2} h(s_3, s_2) \gamma(ds_2|s_1)$ is $\mathcal{T}_{\mathcal{S}_3} \times \mathcal{T}_{\mathcal{S}_1}$ -l.s.c. and bounded from below. If $(\mathcal{S}_3, \mathcal{T}_{\mathcal{S}_3}) = (\mathcal{S}_1, \mathcal{T}_{\mathcal{S}_1})$, it is understood as $\mathcal{T}_{\mathcal{S}_1}$ -l.s.c. and bounded from below;
- (b) with $\lambda \in \mathcal{P}(\mathcal{S}_2)$, $\int_{\mathcal{S}_2} h(s_3, s_2) \lambda(ds_2)$ is $\mathcal{T}_{\mathcal{S}_3} \times \mathcal{V}[C_b(\mathcal{S}_2; \mathcal{T}_{\mathcal{S}_2})]$ -l.s.c. and bounded from below;
- (c) $G(s_1, g(s_2)) : (\mathcal{S}_1 \times \mathcal{S}_2, \mathcal{T}_{\mathcal{S}_1} \times \mathcal{T}_{\mathcal{S}_2}) \rightarrow (\mathbb{R}, \mathcal{T}_{\mathbb{R}})$ is l.s.c.

Proof. By Bertsekas and Shreve (1978, Lemma 7.14), there exists a sequence $h_k(s_3, s_2)$ of continuous and bounded functions such that h_k converges increasingly to h . By monotone convergence theorem,

$$\int_{\mathcal{S}_2} h(s_3, s_2) \gamma(ds_2|s_1) = \int_{\mathcal{S}_2} \sup_k h_k(s_3, s_2) \gamma(ds_2|s_1) = \sup_k \int_{\mathcal{S}_2} h_k(s_3, s_2) \gamma(ds_2|s_1).$$

Hence, claim (a) follows since $\int_{\mathcal{S}_2} h(s_3, s_2) \gamma(ds_2|s_1)$ is a supremum of continuous functions in (s_3, s_1) , by Lemma A.2. Claim (b) can be proved similarly.

For claim (c), we consider a sequence (s_1^n, s_2^n) converging to (s_1, s_2) under the product topology $\mathcal{T}_{\mathcal{S}_1} \times \mathcal{T}_{\mathcal{S}_2}$. Then

$$\liminf_{n \rightarrow \infty} G(s_1^n, g(s_2^n)) \geq \liminf_{n \rightarrow \infty} G(s_1^n, \inf_{k \geq n} g(s_2^k)) \geq G(s_1, \lim_{n \rightarrow \infty} \inf_{k \geq n} g(s_2^k)) \geq G(s_1, g(s_2)).$$

The first inequality uses the fact that $g(s_2^n) \geq \inf_{k \geq n} g(s_2^k)$ and $G(s_1^n, \cdot)$ is nondecreasing. The second inequality holds since $G(\cdot, \cdot)$ is l.s.c. The last inequality is due to $\lim_{n \rightarrow \infty} \inf_{k \geq n} g(s_2^k) = \liminf_{n \rightarrow \infty} g(s_2^n) \geq g(s_2)$. \square

Proof of Corollary 3.5

Proof. The proof is a modification for the case of Theorem 3.3.

Consider time $t = T - 1$. $\nu(dy_T|y_{T-1}) : (\mathcal{Y}_{T-1}, \mathcal{T}_{\mathcal{Y}_{T-1}}^{(1)}) \rightarrow (\mathcal{P}(\mathcal{Y}_T), \mathcal{V}[C_b(\mathcal{Y}_T; \mathcal{T}_{\mathcal{Y}_T})])$ is continuous. By Corollary A.3 and Assumption 3.4, the objective at time $T - 1$, given by

$$f(x_{T-1}, y_{T-1}, \gamma) := \int c_T(x_{T-1}, y_{T-1}, x_T, y_T) \gamma(dx_T, dy_T) + G\left(x_{T-1}, y_{T-1}, \int h(x_T, y_T) \gamma(dx_T, dy_T)\right),$$

is $\mathcal{T}_{\mathcal{X}_{T-1}} \times \mathcal{T}_{\mathcal{Y}_{T-1}}^{(1)} \times \mathcal{V}[C_b(\mathcal{X}_T \times \mathcal{Y}_T; \mathcal{T}_{\mathcal{X}_T} \times \mathcal{T}_{\mathcal{Y}_T})]$ -l.s.c. Indeed, $\int c_T(x_{T-1}, y_{T-1}, x_T, y_T) \gamma(dx_T, dy_T)$ is l.s.c. in $(x_{T-1}, y_{T-1}, \gamma)$ by Corollary A.3 (b). Similarly, $\int h(x_T, y_T) \gamma(dx_T, dy_T)$ is l.s.c. in γ . $G(x_{T-1}, y_{T-1}, \int h(x_T, y_T) \gamma(dx_T, dy_T))$ is l.s.c. in $(x_{T-1}, y_{T-1}, \gamma)$ by Corollary A.3 (c).

There is a Borel measurable optimizer $\pi^*(dx_T, dy_T|x_{T-1}, y_{T-1})$ by Brown and Purves (1973, Corollary 1). It is jointly continuous in (x_{T-1}, y_{T-1}) under a finer product topology $\mathcal{T}_{\mathcal{X}_{T-1}} \times \mathcal{T}_{\mathcal{Y}_{T-1}}^{(n+1)}$ by Kechris (2012, Theorem 13.11). We note that l.s.c. functions are still l.s.c. under a finer topology. Then $g_{T-1}(x_{T-1}, y_{T-1})$ and $b_T(x_i, y_i, x_{T-1}, y_{T-1})$ are still l.s.c. when $\mathcal{X}_{T-1} \times \mathcal{Y}_{T-1}$ is endowed with $\mathcal{T}_{\mathcal{X}_{T-1}} \times \mathcal{T}_{\mathcal{Y}_{T-1}}^{(n+1)}$.

At time $T - 2$, the objective is given by

$$\begin{aligned} f(x_{T-2}, y_{T-2}, \gamma) &:= \int c_{T-1}(x_{T-2}, y_{T-2}, x_{T-1}, y_{T-1}) \gamma(dx_{T-1}, dy_{T-1}) \\ &\quad + G\left(x_{T-2}, y_{T-2}, \int g_{T-1}(x_{T-1}, y_{T-1}) \gamma(dx_{T-1}, dy_{T-1})\right) \\ &\quad + \int b_T(x_{T-2}, y_{T-2}, x_{T-1}, y_{T-1}) \gamma(dx_{T-1}, dy_{T-1}). \end{aligned}$$

It is $\mathcal{T}_{\mathcal{X}_{T-2}} \times \mathcal{T}_{\mathcal{Y}_{T-2}}^{(1)} \times \mathcal{V}[C_b(\mathcal{X}_{T-1} \times \mathcal{Y}_{T-1}; \mathcal{T}_{\mathcal{X}_{T-1}} \times \mathcal{T}_{\mathcal{Y}_{T-1}}^{(n+1)})]$ -l.s.c., by Corollary A.3 and Assumption 3.4. The remaining proof follows similarly as in Theorem 3.3. \square

A.2 The continuous and non-Markovian case

Corollary A.4 extends Lemma A.2 to unbounded functions. We note that Corollary A.4 relies on the metric used to define the growth rate.

Corollary A.4. *Consider metric spaces (\mathcal{S}_1, d_1) , (\mathcal{S}_2, d_2) , and (\mathcal{S}_3, d_3) that are Polish. Moreover, \mathcal{S}_2 is a finite dimensional vector space. With a given $p \in [1, \infty)$, suppose*

- (1) *the stochastic kernel $\gamma(ds_2|s_1) : (\mathcal{S}_1, d_1) \rightarrow \mathcal{P}_p(\mathcal{S}_2)$ is continuous;*
- (2) *the function $h(s_3, s_2) \in C_p(\mathcal{S}_3 \times \mathcal{S}_2)$.*

Then

- (a) $\int_{\mathcal{S}_2} h(s_3, s_2) \gamma(ds_2|s_1)$ *is continuous in (s_3, s_1) ;*
- (b) *if $(\mathcal{S}_3, d_3) = (\mathcal{S}_1, d_1)$ and $\gamma(ds_2|s_1)$ satisfies $\int_{\mathcal{S}_2} d_2(s_2, \bar{s}_2)^p \gamma(ds_2|s_1) \leq C(1 + d_1(s_1, \bar{s}_1)^p)$ for all $s_1 \in \mathcal{S}_1$, then $\int_{\mathcal{S}_2} h(s_1, s_2) \gamma(ds_2|s_1) \in C_p(\mathcal{S}_1)$;*
- (c) *with $\lambda \in \mathcal{P}_p(\mathcal{S}_2)$, $\int_{\mathcal{S}_2} h(s_3, s_2) \lambda(ds_2)$ is continuous in (s_3, λ) .*

Proof. For the claim (a), consider a sequence (s_3^n, s_1^n) converging to (s_3, s_1) . $B := \{(s_3^n, s_1^n)\}_{n=1}^\infty \cup \{(s_3, s_1)\}$ is a compact set. Fix an arbitrary $\varepsilon > 0$. Similar to Lemma A.2, we can find a compact subset $A \subset \mathcal{S}_2$ such that $\sup_n \gamma(\mathcal{S}_2 \setminus A | s_1^n) \leq \varepsilon$. Without loss of generality, we can assume that there is a sufficiently large radius R such that the ball with radius R is contained by A :

$$K_R := \{s_2 | d_2(s_2, \bar{s}_2) \leq R\} \subset A. \quad (\text{A.2})$$

Indeed, since \mathcal{S}_2 is finite dimensional, the closed ball K_R is compact (Charalambos and Aliprantis, 2013, Theorem 5.26). We can use $K_R \cup A$ to replace A if needed.

Similarly, we have

$$\left| \int_{\mathcal{S}_2} h(s_3^n, s_2) \gamma(ds_2|s_1^n) - \int_{\mathcal{S}_2} h(s_3, s_2) \gamma(ds_2|s_1) \right| \leq \text{I} + \text{II} + \text{III},$$

where

$$\begin{aligned} \text{I} &= \left| \int_{\mathcal{S}_2} h(s_3, s_2) [\gamma(ds_2|s_1^n) - \gamma(ds_2|s_1)] \right|, \\ \text{II} &= \left| \int_A [h(s_3^n, s_2) - h(s_3, s_2)] \gamma(ds_2|s_1^n) \right|, \\ \text{III} &= \left| \int_{\mathcal{S}_2 \setminus A} [h(s_3^n, s_2) - h(s_3, s_2)] \gamma(ds_2|s_1^n) \right|. \end{aligned}$$

Since $h(s_3, \cdot)$ satisfies the growth rate condition, then the term I converges to zero when $n \rightarrow \infty$ by Villani (2009, Definition 6.7 (iv)). As the set $B \times A$ is compact, when $n > N$, we have $\text{II} \leq \varepsilon$ by the uniform continuity. For III, since A contains a large enough ball with radius R , then

$$\begin{aligned} \text{III} &\leq \int_{\mathcal{S}_2 \setminus A} (|h(s_3^n, s_2)| + |h(s_3, s_2)|) \gamma(ds_2|s_1^n) \\ &\leq C \sup_n [1 + d_3(s_3^n, \bar{s}_3)^p] \varepsilon + C [1 + d_3(s_3, \bar{s}_3)^p] \varepsilon + 2C \int_{\mathcal{S}_2 \setminus K_R} d_2(s_2, \bar{s}_2)^p \gamma(ds_2|s_1^n). \end{aligned}$$

For the second inequality, we have used the growth rate condition of h , the inequality $\sup_n \gamma(\mathcal{S}_2 \setminus A | s_1^n) \leq \varepsilon$, and the fact that the ball $K_R \subset A$. By Villani (2009, Definition 6.7 (iii)), the last term is less than $2C\varepsilon$ when $n \rightarrow \infty$ and R is sufficiently large. In summary,

$$\limsup_{n \rightarrow \infty} \text{I} + \text{II} + \text{III} \leq C\varepsilon,$$

with a generic constant that is independent of ε . As $\varepsilon > 0$ is arbitrary, we obtain the continuity as desired.

Claim (b) is direct. Claim (c) can be proved similarly to (a). \square

Another useful result is the concatenation of continuous kernels is still continuous.

Corollary A.5. *Consider metric spaces (\mathcal{S}_1, d_1) , (\mathcal{S}_2, d_2) , and (\mathcal{S}_3, d_3) that are Polish. Moreover, \mathcal{S}_2 and \mathcal{S}_3 are finite dimensional vector spaces. With a given $p \in [1, \infty)$, suppose*

- (1) *the stochastic kernel $\pi(ds_2|s_1) : (\mathcal{S}_1, d_1) \rightarrow \mathcal{P}_p(\mathcal{S}_2)$ is continuous and $\int_{\mathcal{S}_2} d_2(s_2, \bar{s}_2)^p \pi(ds_2|s_1) \leq C(1 + d_1(s_1, \bar{s}_1)^p)$;*
- (2) *the stochastic kernel $\pi(ds_3|s_1, s_2) : (\mathcal{S}_1 \times \mathcal{S}_2, (d_1^p + d_2^p)^{1/p}) \rightarrow \mathcal{P}_p(\mathcal{S}_3)$ is continuous and $\int_{\mathcal{S}_3} d_3(s_3, \bar{s}_3)^p \pi(ds_3|s_1, s_2) \leq C(1 + d_1(s_1, \bar{s}_1)^p + d_2(s_2, \bar{s}_2)^p)$.*

Then there exists a unique kernel

$$\pi(ds_{2:3}|s_1) = \pi(ds_3|s_1, s_2)\pi(ds_2|s_1) \quad (\text{A.3})$$

from (\mathcal{S}_1, d_1) to $\mathcal{P}_p(\mathcal{S}_2 \times \mathcal{S}_3)$. It is continuous in s_1 .

Proof. By Bertsekas and Shreve (1978, Proposition 7.28), there exists a unique $\pi(ds_{2:3}|s_1)$ defined by (A.3). We only need to prove the continuity.

Consider a sequence $\{s_1^n\}$ converging to s_1 . By Villani (2009, Definition 6.7 and Theorem 6.8), we need to show that for all continuous functions φ with a growth rate of $|\varphi(s_2, s_3)| \leq C(1 + d_2(s_2, \bar{s}_2)^p + d_3(s_3, \bar{s}_3)^p)$, one has

$$\lim_{n \rightarrow \infty} \int_{\mathcal{S}_2 \times \mathcal{S}_3} \varphi(s_2, s_3) \pi(ds_{2:3}|s_1^n) = \int_{\mathcal{S}_2 \times \mathcal{S}_3} \varphi(s_2, s_3) \pi(ds_{2:3}|s_1). \quad (\text{A.4})$$

By Corollary A.4 (b), $\Phi(s_1^n, s_2) := \int_{\mathcal{S}_3} \varphi(s_2, s_3) \pi(ds_3|s_1^n, s_2)$ is in $C_p(\mathcal{S}_1 \times \mathcal{S}_2)$. Thus, we can apply Corollary A.4 (b) again to $\int_{\mathcal{S}_2} \Phi(s_1^n, s_2) \pi(ds_2|s_1^n)$. It belongs to $C_p(\mathcal{S}_1)$. Then the convergence (A.4) holds. \square

Proof of Theorem 4.4

Proof. The recursive relationship for $V_t(x_{1:t}, y_{1:t})$ in (4.5) is direct. We prove that g_{t+1} and b_{t+1} are continuous and $\theta_{t+1}^*(x_{1:t}, y_{1:t})$ exists.

First, we have $V_T \in C_p(\mathcal{X} \times \mathcal{Y})$ by the boundary condition and Assumption 4.1.

Next, consider time $t = T - 1$. Thanks to Assumption 4.3(1), Assumption 4.1 and Corollary A.4, the objective functional

$$\begin{aligned} f(x_{1:T-1}, y_{1:T-1}, \theta_T) = & G\left(x_{T-1}, y_{T-1}, \int h(x_{1:T}, y_{1:T}) \gamma(dx_T, dy_T | \theta_T)\right) \\ & + \int c(x_{T-1}, y_{T-1}, x_{1:T}, y_{1:T}) \gamma(dx_T, dy_T | \theta_T) \end{aligned}$$

is $\mathcal{T}_{\mathcal{X}_{1:T-1}} \times \mathcal{T}_{\mathcal{Y}_{1:T-1}} \times \mathcal{T}_{\Theta_T}$ -continuous. Moreover, by Assumption 4.3(3), $f(x_{1:T-1}, y_{1:T-1}, \theta_T)$ is strictly quasiconvex in θ_T . Assumption 4.3(2) imposes the required properties of the correspondence D_{T-1} . By a version of Berge's maximum theorem with strict quasiconcavity, see Sundaram (1996, Theorem 9.14 and Corollary 9.20) or Charalambos and Aliprantis (2013, Theorem 17.31), V_{T-1} given by

$$V_{T-1}(x_{1:T-1}, y_{1:T-1}) = \inf_{\theta_T \in D_{T-1}(x_{1:T-1}, y_{1:T-1})} f(x_{1:T-1}, y_{1:T-1}, \theta_T)$$

is $\mathcal{T}_{\mathcal{X}_{1:T-1}} \times \mathcal{T}_{\mathcal{Y}_{1:T-1}}$ -continuous and the infimum is attained. There exists a unique and continuous optimizer $\theta_T^*(x_{1:T-1}, y_{1:T-1}) : (\mathcal{X}_{1:T-1} \times \mathcal{Y}_{1:T-1}, d) \rightarrow (\Theta_T, d_{\Theta_T})$, which is a function instead of correspondence. As a composition, $\gamma(dx_T, dy_T | \theta_T^*(x_{1:T-1}, y_{1:T-1})) : (\mathcal{X}_{1:T-1} \times \mathcal{Y}_{1:T-1}, d) \rightarrow \mathcal{P}_p(\mathcal{X}_T \times \mathcal{Y}_T)$ is also continuous.

For the growth rate, we note the marginal constraint

$$\gamma(dx_T, dy_T | \theta_T^*(x_{1:T-1}, y_{1:T-1})) \in \Pi(\mu(dx_T | x_{1:T-1}), \nu(dy_T | y_{1:T-1}))$$

together with Assumption 4.2 (2). Then

$$\begin{aligned} & \left| \int_{\mathcal{X}_T \times \mathcal{Y}_T} c(x_{T-1}, y_{T-1}, x_{1:T}, y_{1:T}) \gamma(dx_T, dy_T | \theta_T^*(x_{1:T-1}, y_{1:T-1})) \right| \\ & \leq \int_{\mathcal{X}_T \times \mathcal{Y}_T} C \left[1 + \sum_{t=1}^T d_{\mathcal{X}_t}(x_t, \bar{x}_t)^p + \sum_{t=1}^T d_{\mathcal{Y}_t}(y_t, \bar{y}_t)^p \right] \gamma(dx_T, dy_T | \theta_T^*(x_{1:T-1}, y_{1:T-1})) \\ & = C + C \int_{\mathcal{X}_T} \sum_{t=1}^T d_{\mathcal{X}_t}(x_t, \bar{x}_t)^p \mu(dx_T | x_{1:T-1}) + C \int_{\mathcal{Y}_T} \sum_{t=1}^T d_{\mathcal{Y}_t}(y_t, \bar{y}_t)^p \nu(dy_T | y_{1:T-1}) \\ & \leq C \left[1 + \sum_{t=1}^{T-1} d_{\mathcal{X}_t}(x_t, \bar{x}_t)^p + \sum_{t=1}^{T-1} d_{\mathcal{Y}_t}(y_t, \bar{y}_t)^p \right]. \end{aligned}$$

Similarly, with Assumption 4.1, one has

$$\begin{aligned} & \left| G \left(x_{T-1}, y_{T-1}, \int_{\mathcal{X}_T \times \mathcal{Y}_T} h(x_{1:T}, y_{1:T}) \gamma(dx_T, dy_T | \theta_T^*(x_{1:T-1}, y_{1:T-1})) \right) \right| \tag{A.5} \\ & \leq C \left(1 + \left| \int_{\mathcal{X}_T \times \mathcal{Y}_T} h(x_{1:T}, y_{1:T}) \gamma(dx_T, dy_T | \theta_T^*(x_{1:T-1}, y_{1:T-1})) \right|^{pr} + d((x_{T-1}, y_{T-1}), (\bar{x}_{T-1}, \bar{y}_{T-1}))^p \right) \\ & \leq C \left(1 + \int_{\mathcal{X}_T \times \mathcal{Y}_T} |h(x_{1:T}, y_{1:T})|^{pr} \gamma(dx_T, dy_T | \theta_T^*(x_{1:T-1}, y_{1:T-1})) + d((x_{T-1}, y_{T-1}), (\bar{x}_{T-1}, \bar{y}_{T-1}))^p \right) \\ & \leq C [1 + d((x_{1:T-1}, y_{1:T-1}), (\bar{x}_{1:T-1}, \bar{y}_{1:T-1}))^p]. \end{aligned}$$

Therefore, $V_{T-1} \in C_p(\mathcal{X}_{1:T-1} \times \mathcal{Y}_{1:T-1})$.

By Corollary A.4 and $1/r \leq p$, the following functions are continuous in $(x_{1:T-1}, y_{1:T-1})$:

$$\begin{aligned} g_{T-1}(x_{1:T-1}, y_{1:T-1}) &:= \int h(x_{1:T}, y_{1:T}) \gamma(dx_T, dy_T | \theta_T^*(x_{1:T-1}, y_{1:T-1})), \\ b_{T-1}(x_i, y_i, x_{1:T-1}, y_{1:T-1}) &:= \int c(x_i, y_i, x_{1:T}, y_{1:T}) \gamma(dx_T, dy_T | \theta_T^*(x_{1:T-1}, y_{1:T-1})), \quad i \in \{0, \dots, T-1\}. \end{aligned}$$

In each step of backward induction, we also use Corollary A.5 that the successive concatenation of continuous conditional kernels $\gamma(dx_T, dy_T | \theta_T^*(x_{1:T-1}, y_{1:T-1})), \dots, \gamma(dx_{t+1}, dy_{t+1} | \theta_{t+1}^*(x_{1:t}, y_{1:t}))$ induces a unique continuous conditional probability measure $\gamma(dx_{t+1:T}, dy_{t+1:T} | \theta_{t+1:T}^*(x_{1:t}, y_{1:t}))$. \square

Proof of Corollary 4.6

With $\Theta_{t+1} = \mathcal{P}_p(\mathcal{X}_{t+1} \times \mathcal{Y}_{t+1})$, we only need to show the correspondence D_t satisfies Assumption 4.3 (2) in Corollary A.6. Then Corollary 4.6 follows directly from Theorem 4.4. Compared with Neufeld and Sester (2021), Corollary A.6 considers the W_p metric and do not have martingale constraints.

Denote the sum of Wasserstein distances between $\mu, \mu' \in \mathcal{P}(\mathcal{X})$ and $\nu, \nu' \in \mathcal{P}(\mathcal{Y})$ as

$$W_p^\oplus((\mu, \nu), (\mu', \nu')) := W_p(\mu, \mu') + W_p(\nu, \nu').$$

Corollary A.6. *Consider the metric spaces and Wasserstein distances in Section 4.1. For a given t , denote a correspondence as*

$$D : \mathcal{X}_{1:t} \times \mathcal{Y}_{1:t} \rightharpoonup \mathcal{P}_p(\mathcal{X}_{t+1} \times \mathcal{Y}_{t+1}) \text{ that maps } (x_{1:t}, y_{1:t}) \mapsto \Pi(\mu(dx_{t+1}|x_{1:t}), \nu(dy_{t+1}|y_{1:t})).$$

Suppose Assumption 4.2 Condition (1) holds. Then D is a continuous correspondence with non-empty, convex, and compact images, under the product topology of $\mathcal{T}_{\mathcal{X}_{1:t}}$, $\mathcal{T}_{\mathcal{Y}_{1:t}}$, and the topology induced by the Wasserstein distance on $\mathcal{P}_p(\mathcal{X}_{t+1} \times \mathcal{Y}_{t+1})$.

Proof. With the metric d on $\mathcal{X}_{1:t} \times \mathcal{Y}_{1:t}$ and the metric W_p on $\mathcal{P}_p(\mathcal{X}_{t+1})$, $\mathcal{P}_p(\mathcal{Y}_{t+1})$, and $\mathcal{P}_p(\mathcal{X}_{t+1} \times \mathcal{Y}_{t+1})$, we first show that the correspondence $(\alpha, \beta) \mapsto \Pi(\alpha, \beta)$ is continuous with W_p^\oplus metric on the domain and W_p on the range.

Compactness and upper hemicontinuity: The idea is similar to Lemma A.1. We show that if a sequence $\{(\alpha^n, \beta^n, \gamma^n)\}$ is in the graph of D and

$$\lim_{n \rightarrow \infty} W_p^\oplus((\alpha^n, \beta^n), (\alpha, \beta)) = 0, \quad (\text{A.6})$$

then the sequence $\{\gamma^n\}$ has a limit point in $\Pi(\alpha, \beta)$.

By Villani (2009, Definition 6.7), the convergence in (A.6) implies the usual weak convergence. With the same argument in Lemma A.1, we can prove that a subsequence $\{\gamma^{n_k}\}_{k=1}^\infty$ converges weakly in the usual sense to some $\gamma \in \Pi(\alpha, \beta)$. Furthermore,

$$\begin{aligned} & \lim_{k \rightarrow \infty} \int_{\mathcal{X}_{t+1} \times \mathcal{Y}_{t+1}} d((x_{t+1}, y_{t+1}), (\bar{x}_{t+1}, \bar{y}_{t+1}))^p \gamma^{n_k}(dx_{t+1}, dy_{t+1}) \\ &= \lim_{k \rightarrow \infty} \int_{\mathcal{X}_{t+1} \times \mathcal{Y}_{t+1}} [d\mathcal{X}_{t+1}(x_{t+1}, \bar{x}_{t+1})^p + d\mathcal{Y}_{t+1}(y_{t+1}, \bar{y}_{t+1})^p] \gamma^{n_k}(dx_{t+1}, dy_{t+1}) \\ &= \lim_{k \rightarrow \infty} \left(\int_{\mathcal{X}_{t+1}} d\mathcal{X}_{t+1}(x_{t+1}, \bar{x}_{t+1})^p \alpha^{n_k}(dx_{t+1}) + \int_{\mathcal{Y}_{t+1}} d\mathcal{Y}_{t+1}(y_{t+1}, \bar{y}_{t+1})^p \beta^{n_k}(dy_{t+1}) \right) \\ &= \int_{\mathcal{X}_{t+1}} d\mathcal{X}_{t+1}(x_{t+1}, \bar{x}_{t+1})^p \alpha(dx_{t+1}) + \int_{\mathcal{Y}_{t+1}} d\mathcal{Y}_{t+1}(y_{t+1}, \bar{y}_{t+1})^p \beta(dy_{t+1}) \\ &= \int_{\mathcal{X}_{t+1} \times \mathcal{Y}_{t+1}} [d\mathcal{X}_{t+1}(x_{t+1}, \bar{x}_{t+1})^p + d\mathcal{Y}_{t+1}(y_{t+1}, \bar{y}_{t+1})^p] \gamma(dx_{t+1}, dy_{t+1}) \\ &= \int_{\mathcal{X}_{t+1} \times \mathcal{Y}_{t+1}} d((x_{t+1}, y_{t+1}), (\bar{x}_{t+1}, \bar{y}_{t+1}))^p \gamma(dx_{t+1}, dy_{t+1}). \end{aligned}$$

Therefore, conditions in Villani (2009, Definition 6.7 (i)) are verified and we obtain the convergence $\lim_{k \rightarrow \infty} W_p(\gamma^{n_k}, \gamma) = 0$.

Lower hemicontinuity: By Charalambos and Aliprantis (2013, Theorem 17.21), we have to prove the following claim: For any $(\alpha, \beta) \in \mathcal{P}_p(\mathcal{X}_{t+1}) \times \mathcal{P}_p(\mathcal{Y}_{t+1})$, if (α^n, β^n) converges weakly to

(α, β) in the metric W_p^\oplus , then for each $\gamma \in \Pi(\alpha, \beta)$, there exists a subsequence $(\alpha^{n_k}, \beta^{n_k})$ and $\gamma^k \in \Pi(\alpha^{n_k}, \beta^{n_k})$ for each k , such that γ^k converges weakly to γ in $\mathcal{P}_p(\mathcal{X}_{t+1} \times \mathcal{Y}_{t+1})$ (Villani, 2009, Definition 6.7). Indeed, this result has been proved in Beiglböck et al. (2022, Equations 2.1 and 2.2).

We have proved the continuity of the correspondence $(\alpha, \beta) \mapsto \Pi(\alpha, \beta)$ and the compactness of the images. Moreover, Assumption 4.2 Condition (1) guarantees that $(x_{1:t}, y_{1:t}) \mapsto (\mu(dx_{t+1}|x_{1:t}), \nu(dy_{t+1}|y_{1:t}))$ is continuous. By Charalambos and Aliprantis (2013, Theorem 17.23) on the continuity of the composition of correspondence, D , viewed as the composition

$$(x_{1:t}, y_{1:t}) \mapsto (\mu(dx_{t+1}|x_{1:t}), \nu(dy_{t+1}|y_{1:t})) \mapsto \Pi(\mu(dx_{t+1}|x_{1:t}), \nu(dy_{t+1}|y_{1:t})),$$

is also continuous. □

B Supplement to the executive job market

B.1 Data cleaning and summary statistics

The choice of a five-year time horizon 2017 – 2021 is motivated by the following factors. A longer time horizon incurs a heavy computational burden. Moreover, in our final dataset, the median tenure of a CEO is 4 years and the average tenure is 5.97 years. In the literature with different datasets, Taylor (2013, Table 1) reported the average CEO tenure as 7.9 years and the median as 6 years. Overall, a five-year time horizon is close to the CEO’s tenure. Besides, the job market can change significantly over a longer period.

To obtain and clean the data, we adopt the following steps:

1. We download the net sales data from Compustat and the executive compensation information from Execucomp. There are no restrictions on the net sales or market values of firms at this stage. The key variables are net sales (“sale” in Compustat) and total compensation (“tdc1” in Execucomp). In 2017 – 2021, we have data on 1998 firms from Execucomp and 11911 firms from Compustat. Execucomp primarily includes salary information for S&P 1500 components.
2. We remove firms with missing net sales data for the five-year period. Compensation data are usually available for the CEO, chief financial officer, and the three other most highly compensated executive officers. We use their mean salary as the representative wage paid to top executives by the firm. After merging the sale and wage datasets, there are 1590 firms remaining.
3. To further filter the firms, we restrict our analysis to companies with investment-grade credit ratings. We download the S&P Domestic Long-Term Issuer Credit Rating (variable name: “splticrm”) and remove firms with a rating of CCC+ or lower. We also remove firms without ratings.

Table 7 shows the descriptive statistics for the data.

B.2 Estimated transition matrices

Figure 7 gives the estimated transition matrices for sale and wage ranks. Group 1 is the group with the highest wages or sales. To save space, we average the transition matrices across 11 sectors and summarize them in two figures. A common pattern in all sectors is that sale ranks are more stable than wage ranks. Wages are more stable for the highest and the lowest group. For the wage groups in the middle, the probability of a rise or fall in wage ranks is approximately equal.

B.3 Robustness check with different number of clusters

As a robustness check, we examine the results in Section 6 with different numbers of clusters. The screening method in Figure 2b suggests that the choice of five clusters is also reasonable. All other specifications are kept the same. The first row of Table 8 shows that the systematic bias moves further toward the negative side as the number of clusters decreases, indicating that the outcomes may be more similar to the one-cluster case. When resampled real data are used, we obtain the same conclusion as in the six-cluster situation. Table 9 finds that the correlations are negative and the p -values are smaller than 5%.

When seven clusters are used, the systematic bias shifts to the positive side, as shown in the first row of Table 10. The original and adjusted optimal α tend to be larger than those obtained

Industry	GICS Code	Number of firms	Market value	Net sales	Compensation
Energy	10	48	22693.93	19713.07	4.82
Materials	15	66	12889.25	7301.68	3.79
Industrials	20	118	20781.59	12368.6	4.14
Consumer Discretionary	25	112	32048.23	16761.5	5.80
Consumer Staples	30	48	46617.8	34468.41	5.55
Health Care	35	63	51570.67	33801.81	6.07
Financials	40	110	24242.18	16041.93	5.38
Information Technology	45	79	75539.2	17750.21	7.25
Communication Services	50	30	78888.99	26807.29	9.02
Utilities	55	50	18192.87	7446.87	3.21
Real Estate	60	66	11529.68	1949.91	3.88

Table 7: Summary statistics of firms over 2017 – 2021. Values in the last three columns are measured in millions of USD.

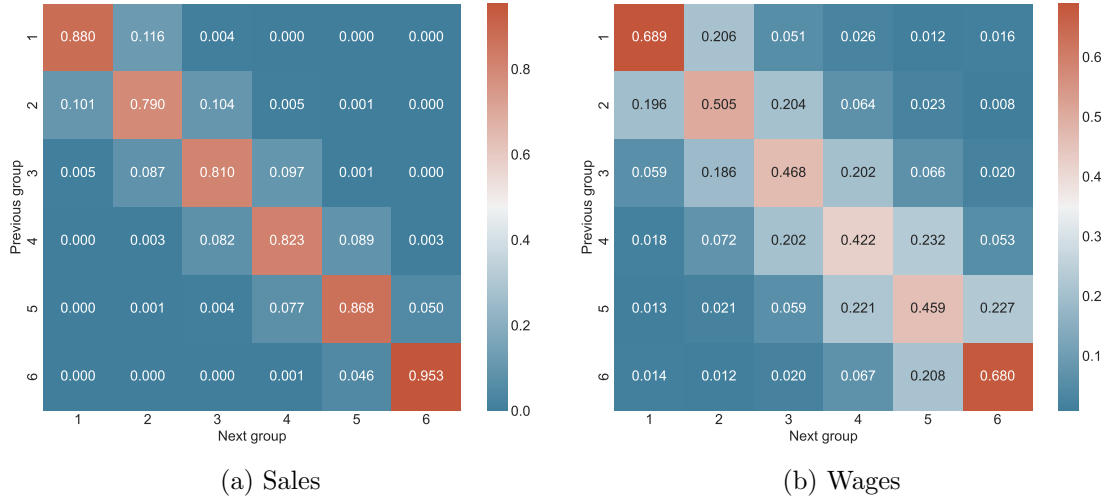


Figure 7: Transition matrices of wage and sale ranks. The matrices are averaged across 11 sectors.

Sector	10	15	20	25	30	35	40	45	50	55	60
Benchmark α	-0.42	-0.12	-0.318	-0.324	-0.282	-0.366	-0.42	-0.21	-0.252	-0.222	-0.294
Raw α	0.012	-0.072	-0.006	0.45	-0.132	-0.51	-0.444	-0.066	-0.492	-0.462	0.054
Adjusted α	0.432	0.048	0.312	0.774	0.15	-0.144	-0.024	0.144	-0.24	-0.24	0.348

Table 8: Mean values of the optimal α using five clusters. Other settings are the same as in the six-cluster counterpart.

Correlation	Spearman (p -value)	Kendall (p -value)
Raw α	−0.709 (0.015)	−0.636 (0.006)
Adjusted α	−0.700 (0.016)	−0.636 (0.006)

Table 9: Testing the association between job market efficiency and inertia when five clusters are adopted.

Sector	10	15	20	25	30	35	40	45	50	55	60
Benchmark α	0.234	−0.06	0.33	0.324	−0.06	0.582	−0.096	0.198	−0.102	0.066	0.078
Raw α	0.372	−0.06	0.756	0.42	0.222	0.636	0.054	0.438	0.204	0.264	0.666
Adjusted α	0.138	0.0	0.426	0.096	0.282	0.054	0.15	0.24	0.306	0.198	0.588

Table 10: Mean values of the optimal α using seven clusters. Other settings are the same as in the six-cluster counterpart.

using five or six clusters. Although the correlations in Table 11 are still negative, the power of the test is much lower. One possible explanation is that Figure 2b shows that the choice of seven clusters results in a slightly worse correlation than the five and six clusters options. In addition, estimation errors in the transition matrices can be larger. Unfortunately, using a longer period of empirical data to estimate the transition matrices may not be a viable solution, as the job market may not be stationary over a long time horizon. Our parameter settings were fine-tuned for six clusters, so it is expected that the performance can be worse with a different number of clusters.

C Supplement to the academic job market

C.1 Summary statistics

University	Number of employees	Min wage	Median wage	Max wage
UC Berkeley	222	3000.0	250141.5	632257.0
UC Davis	164	1250.0	211538.0	472937.0
UC Irvine	172	2117.0	225990.0	609000.0
UC Los Angeles	195	1906.0	330058.0	778102.0
UC Merced	29	19401.0	207291.5	350160.0
UC Riverside	72	500.0	230418.5	412552.0
UC San Diego	181	12400.0	246321.0	586884.0
UC Santa Barbara	114	21667.0	258774.0	580967.0
UC Santa Cruz	66	6936.0	182750.0	379110.0

Table 12: Wage statistics of B/E/E professors in 2017 – 2021. The numbers of employees are in 2021 only. Min, median, and max wages (in U.S. dollars) are for five years from 2017 to 2021.

Correlation	Spearman (p -value)	Kendall (p -value)
Raw α	−0.345 (0.298)	−0.382 (0.121)
Adjusted α	−0.245 (0.467)	−0.309 (0.218)

Table 11: Testing the association between job market efficiency and inertia when seven clusters are adopted.

University	Number of employees	Min wage	Median wage	Max wage
UC Berkeley	73	11086.0	209901.0	582942.0
UC Davis	49	54768.0	160465.0	313901.0
UC Irvine	64	45856.0	171821.0	387084.0
UC Los Angeles	40	4057.0	261654.0	494989.0
UC Merced	27	62208.0	155763.0	230762.0
UC Riverside	44	10608.0	175183.0	301166.0
UC San Diego	60	11258.0	199728.0	436367.0
UC Santa Barbara	13	36633.0	176921.0	430169.0
UC Santa Cruz	22	10667.0	163482.0	235600.0

Table 13: Wage statistics of B/E/E associate professors. Numbers are reported in the same way as in Table 12.

University	Number of employees	Min wage	Median wage	Max wage
UC Berkeley	72	9992.0	172602.5	356679.0
UC Davis	51	1000.0	141866.0	262833.0
UC Irvine	74	10833.0	143116.0	331450.0
UC Los Angeles	82	8917.0	175874.5	408104.0
UC Merced	31	8450.0	129069.0	203730.0
UC Riverside	58	27775.0	132105.5	266866.0
UC San Diego	97	2386.0	155516.0	429625.0
UC Santa Barbara	48	1295.0	162483.0	302019.0
UC Santa Cruz	45	9017.0	138514.0	247281.0

Table 14: Wage statistics of B/E/E associate professors. Numbers are reported in the same way as in Table 12.

University	Number of employees	Min wage	Median wage	Max wage
UC Berkeley	1246	4.0	44151.0	197419.0
UC Davis	933	2.0	45978.0	137724.0
UC Irvine	524	40.0	43032.0	102079.0
UC Los Angeles	1056	10.0	48566.0	181982.0
UC Merced	89	1694.0	39271.5	100772.0
UC Riverside	299	42.0	44651.0	87372.0
UC San Diego	1394	14.0	46350.0	139683.0
UC Santa Barbara	430	54.0	47104.0	148142.0
UC Santa Cruz	184	106.0	45629.5	80133.0

Table 15: Wage statistics of postdocs. Numbers are reported in the same way as in Table 12.

C.2 Estimated transition matrices

To estimate the transition matrices of wages and university rankings, we use data from 2013 to 2021, the longest period available for UC employee salaries on the Government Compensation in California website. Figure 8 shows that university rankings are stable in this time horizon. Most university ranking transitions happen between the second and the third group. For wages, Figure

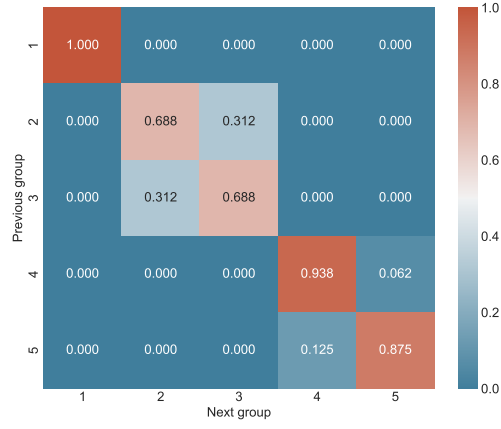
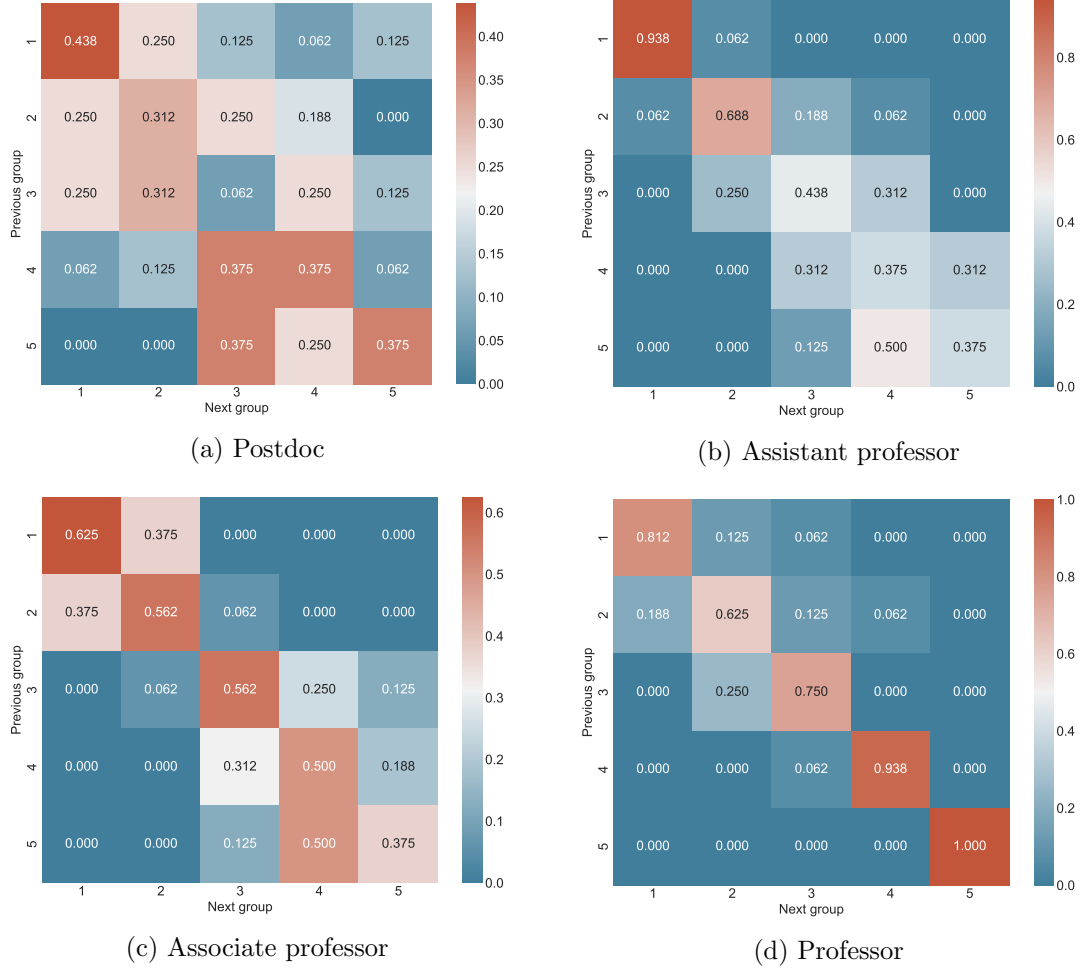


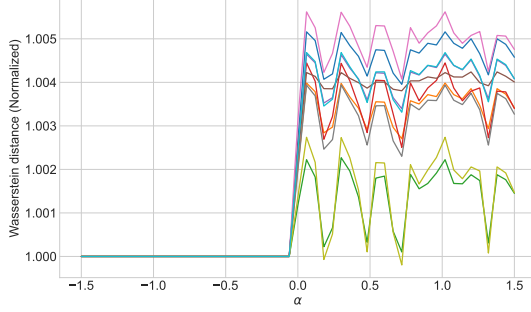
Figure 8: Transition matrices of university rankings.

Figure 9: Transition matrices of wages.

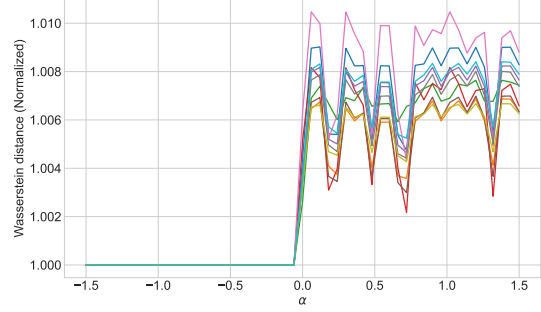


9 demonstrates that postdoc wage ranks are relatively unstable over time. The transition matrices become more and more stable when the academic job ranks become higher. The first group with the highest wages is stable among tenure-track and tenured faculty, while it is unstable for postdoc employees.

C.3 Calibration curves for assistant and associate professors

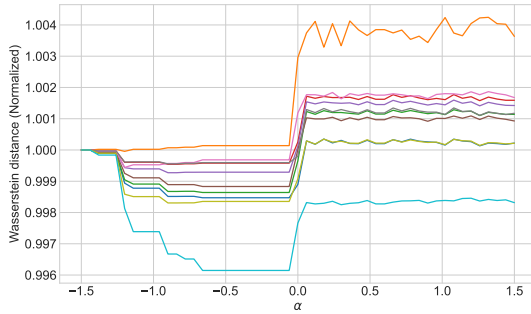


(a) Synthetic data with perfect matching

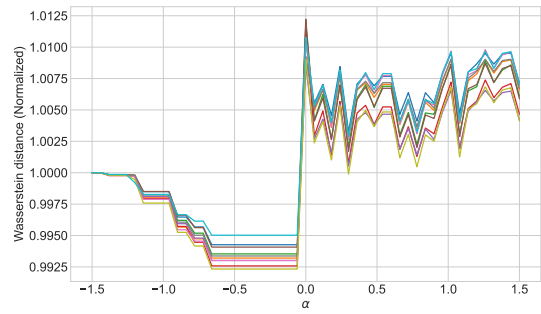


(b) Resampled real data

Figure 10: Calibration curves for B/E/E assistant professors.



(a) Synthetic data with perfect matching



(b) Resampled real data

Figure 11: Calibration curves for B/E/E associate professors.